97p.

Related Report
N62-16864

SUI 62-14

UNPUBLISHED PRELIMINARY DATA

[redacted]

NsG-233-62

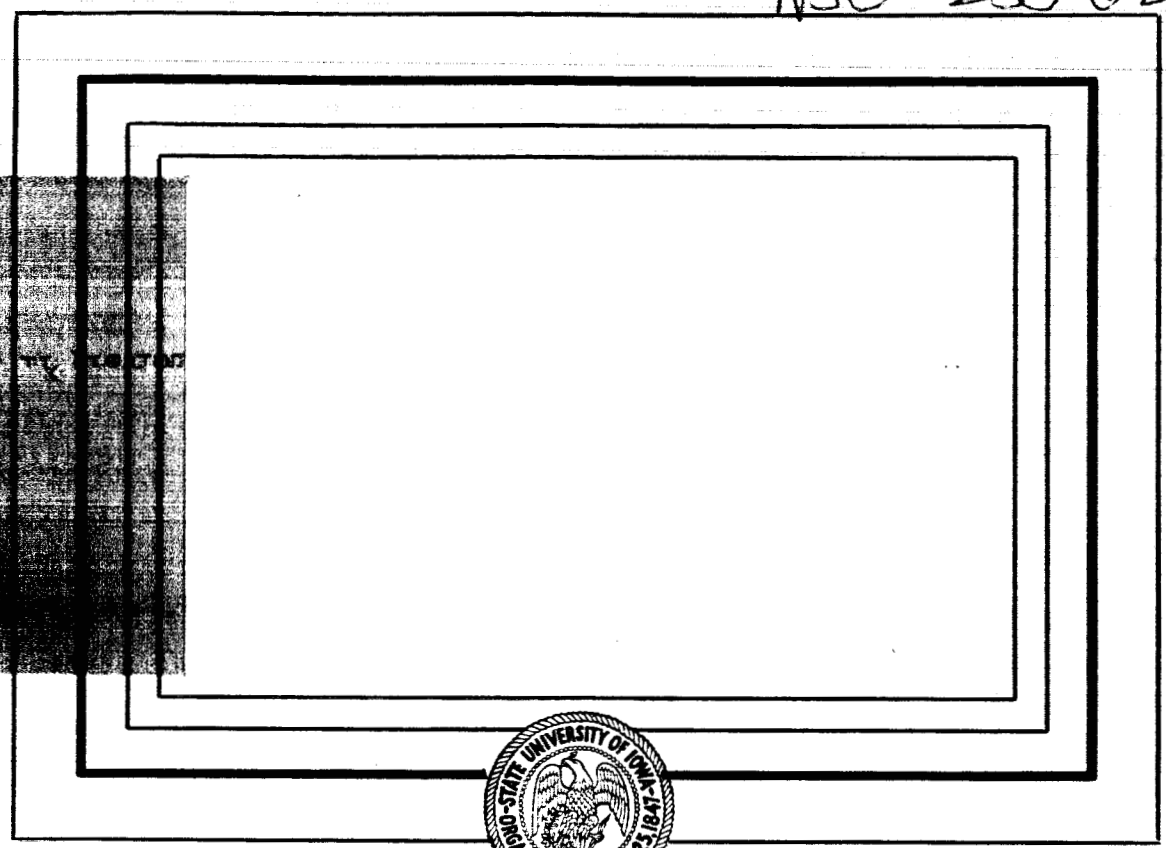

OTS PRICE

XEROX $ 8.60 pl

MICROFILM $ 3.11 mf

Department of Physics and Astronomy

STATE UNIVERSITY OF IOWA

Iowa City, Iowa

A STUDY OF THE AURORA AUSTRALIS IN CONNECTION WITH AN ASSOCIATION BETWEEN VLFE HISS AND AURORAL ARCS AND BANDS OBSERVED AT SOUTH GEOGRAPHICAL POLE 1960

Henry M. Morozumi

A thesis submitted in partial fulfillment of the requirements for the degree of Master of Science in the Department of Physics and Astronomy in the Graduate College of the State University of Iowa

August 1962

Chairman: Professor Brian J. O'Brien

ACKNOWLEDGEMENTS

The observational equipment was provided by the Air Force Cambridge Research Laboratory (AFCRL) and the State University of Iowa (SUI), Department of Physics and Astronomy.

I am indebted to Dr. Helliwell of Stanford University for his permission to use the VLF equipment. Hiss audio spectra were provided by the Radioscience Laboratory, Stanford University. I wish to thank Messrs. Morse of National Bureau of Standards (NBS), Flowers of United States Weather Bureau (USWB), Oliver of AFCRL, and Goodwin of United States Coast and Geodetic Survey (USC and GS) for making the data available.

I wish to thank Professor Gartlein of the World Data Center A (WDC-A), Cornell University, for proposing the IBM analysis. I am particularly indebted to Dr. Sprague for his many suggestions and help in IBM operation and the computation of Tables I and II. Mrs. Clark of Cornell University kindly provided Figures 4, 5, and 6 from her thesis.

The research was done at AFCRL, Cornell WDC-A, and the State University of Iowa. Discussions with Messrs. B. Sanford, T. Obayashi, R. Gallet, B. Maehlum, and many associates in this

university were valuable in improving this material. I am greatly indebted to my advisor, Dr. B. J. O'Brien, for his many suggestions. It is my pleasure to acknowledge Dr. J. A. Van Allen's interest in this thesis project at this university.

The author also wishes to thank Mrs. DeLong, Mr. Jump, and Miss Van Dusen of WDC-A, and Mrs. Robison of SUI for their assistance.

Most of the research was supported by the Arctic Institute of North America, and partly by the State University of Iowa and USARP, National Science Foundation.

TABLE OF CONTENTS

TABLE OF FIGURES

TABLE OF FIGURES (continued)

TABLE OF ILLUSTRATIONS

TABLE OF TABLES

ABSTRACT

Observations of auroras and VLF hiss were made during the dark months of 1960 at the South Pole. About one thousand hours of auroral observations were made. The data were analyzed statistically on the IBM 101 computer from 3432 cards. In the analysis detailed studies were also made of more than three thousand hours of data from photometers, magnetometers, an all sky camera, and a VLF receiver.

A close association between VLF hiss and auroral arcs and bands was found, which had a diurnal occurrence peak at a few hours before the magnetic midnight. Less identifiable long ray type aurora diurnal peak was found at around a few hours before the magnetic noon. These two types of auroras were markedly different in various aspects. The differences are discussed in this thesis. A brief theoretical consideration on the VLF emission mechanism is given.

I. INTRODUCTION

Although the existence of naturally occurring audio-frequency electromagnetic waves had been reported by several authors, Burton and Boardman [1933] appear to be the first to have observed any correlation between such emissions and various geophysical disturbances. They reported a correlation between atmospherics and auroral activity. The frequency range of their receiving equipment was 150 to 4000 cps.

Various researchers have studied atmospherics and cosmic radio noises since then. Such radio emissions were found to be distributed over a wide spectral range, not only in the kilocycle range but up to several megacycles or higher. Some workers investigated the nature of noise in the megacycle region [Shain, 1954; Ellis, 1956; and Ellis, 1957a]. The original purpose of researches in the megacycle region, however, was mainly the study of radio galaxies [Shklovsky, 1960]. Menzel and others developed their theories and observed the phenomena in ELF-VLF region, seeking correlation between the low frequency radio emission and changes in the earth's magnetic field, etc. [Aarons et al., 1953, 1956; Menzel et al., 1948; and Willis, 1948]. The work of Storey identified some of the audio-frequency signals as whistlers, inferring the electromagnetic wave emission from

lightning, which propagated through the exosphere by means of a quasi-longitudinal mode. There are other types of emissions which are independent of thunderstorm activity /Ellis, 1959; and Gallet, 1959/, such as stated by Burton and others. A close correlation was found between solar activity and the electromagnetic emission of a second type in the frequency range between 2 and 10 kc/s /Ellis, 1960/. Such radio wave emission is generally called VLFE, very low frequency emission. No widely accepted definitions of VLF, ELF, and micropulsation frequency ranges are in use. However, we are tending to use 1cps as the upper frequency of micropulsations and 1 - 3000 cps for the ELF range, and 3000 - 30,000 cps for the VLF range /Helliwell, 1962b/. Among the many kinds of VLFE /Aarons, 1956, 1960; Ellis, 1957; Gallet, 1959; Martin et al., 1960; and Allcock, 1957/ a certain type of emission identified as "hiss" has received attention recently /Watts, 1957/. Some evidence has been found on associations between hiss and various geophysical phenomena /Aarons, 1960; Ellis, 1960a and 1960b; Martin et al., 1960; Watts, 1957; and Helliwell, et al., 1962a/.

Watts reported his observation of "hiss" on March 3, 1956, recorded at Boulder, Colorado, as follows:

> An observer arrived at the field station to find another signal which was different from whistlers and

> choruses, a loud hissing noise, being recorded. The energy was obviously enormous, since the needle of the tape recorded level meter, normally near zero end of the scale except for the atmospherics, was pinned continuously against the top stop.

Such noise lasted more than twelve hours. Gallet observed more than ten hours' hiss; however, he found the average duration to be 1.6 hours for 122 distinct cases [1959]. A relationship was found between 2130 kc/s cosmic noise and E_s [Ellis, 1957a]. Ellis found approximately 50 per cent of isolated noise bursts may be correlated with magnetic bays [Ellis, 1960b]. Correlations between the VLFE and magnetic phenomena are reported elsewhere [Watts, 1957]. The physical dimension of the audio-electromagnetic wave emitter was measured recently [Ellis, 1961]. Simultaneous observations of sub-visual aurora and radio noise on 4.6 kc/s were made by Ellis [1959]. An association was found between hiss and the aurora at Byrd Station and a diurnal variation of both events was shown statistically [Martin et al., 1960]. A correlation study of the same nature at lower latitude has not been as successful [Gartlein et al., 1960]. In any case, there has been no one-to-one systematic study of VLF hiss and various types of aurora.

Theories of emission mechanisms have been developed by several authors [Ellis, 1957b; Gallet, 1959; Allcock, 1957; Aarons, 1960; Ondoh, 1961; and Chamberlain, 1961]. Meinel

observed the incoming hydrogen, and recently Van Allen [1961] discovered zones of highly energetic particles around the earth. Inferring from theories [Stomer, 1955; and Kern et al., 1961], the VLFE may have a relationship to these highly energetic particles and consequently to the cause of the primary excitation of auroras. The purpose of this paper is to show how VLFE hiss is related to the various geophysical phenomena, especially to the aurora, based on the synoptic observations made by the author to the South Geographical Pole, during the Austral winter, 1960.

II. INSTRUMENTATION FOR THE OBSERVATION

1.

This chapter will explain various instruments which were used for the observation.

Six detectors were operated simultaneously. There were three photometers, an electronic direct reading magnetometer, a VLF radio receiver, and the cosmic ray monitor. We do not make use of cosmic-ray data in the studies discussed here.

We used two different recorder systems, having the following purposes in mind. The first purpose was to run the recorder continuously throughout the season with very low speed in order to obtain a gross behavior of events. The second purpose was to magnify special events to see fine detail without disturbing the continuous recordings. Therefore, the Esterline Angus recorder was run with a paper speed of 3/4 inches per hour to study general correlations. A Brush DC recorder was used with paper speed of 1 mm/sec to magnify special events. In this way, we did not waste recording paper, since we turned on the fast speed recorder only when it was necessary. Figure 1 shows the block diagram of the above described system.

2.

Visual Program

Visual observations of aurora were carried out according to the standard IGY method, with some modifications /Gartlein et al., 1957/.

Figure 2 shows orientation of various instruments on the roof of the aurora tower. The location of an alidide was accurately measured by Mr. Goodwin of USC and GS prior to the aurora season. Figure 3 shows the exact location of the aurora tower relative to the magnetic and Greenwich meridians.

In order to measure the elevation and azimuthal angle of aurora accurately, we used alidide cards /Kimball et al., 1957/, which is shown in Figure 4 /Clark, 1961/. Assuming the average height of the aurora to be 100 km /Stomer, 1955/, the elevation angle was converted into a linear distance from the observer, Figure 5 /Clark, 1961/. Figure 6 shows the latest auroral isochasm. Note that South Pole is almost on the maximum auroral frequency line /Clark, 1961/.

Earphones from the VLF receiver were wired to the visual dome, where a written log was kept by a dim-light-equipped pen during the observation. Intercom helped contacts from the aurora office.

During the aurora season the plexiglass dome was often troubled with frost in the Antarctic observatory. A new dome defrosting mechanism was devised, which somewhat eased the problem. Essentially, the system involves a forced circulation of air inside the visual dome.

3.

All Sky Camera

The standard 16-mm black-and-white All Sky camera [Elvey et al., 1957] was operated without a plexiglass dome.

The All Sky camera holder was devised in order to be able to dismount the camera in case of a major breakdown during the season.

We began the operation on April 16, 1960, when the sun was 10° below the horizon. Exposures were 70-20-5 [Elvey et al., 1957]. During the season the new plane mirror heater did not seem to put out enough heat so that it was necessary to clean the surface of the mirror when the temperature was below 85° F. Drifting snow often accumulated on the binary number box.

Since the arc lamp wire was replaced by a cold temperature wire, there was no trouble during the season.

The 5577 interference filter of band width 50 Å was placed in front of the K-100 camera lens on August 28 to extend the

operational period, since the filter eliminated most of the scattered solar continuum. All the indicator lamp voltages had to be readjusted. The operation stopped on September 9 when the sun was at 5° N.

4.

Photometer

The Photometers in General.

Three photometers have been operated at the South Pole station since the winter of 1960. They are meridian, directional, and the All Sky photometer. Photometric measurement of the aurora light is facilitated at the South Pole more than other geographical locations due to the continuous darkness in winter.

Various experiments were attempted by using interference filters with peak transmissions at 3914, 4861, 5577, and 6300 Angstrom.

Meridian Photometer.

Since the spectrograph exposures were controlled by a programmed timer during the winter night, the spectrograph photometer circuit was connected to the cathode follower to record the auroral light along the magnetic meridian. The aperture of the

photometer optics was 2 x 180°. Integrator input was modified in order to record the photometer output throughout the season. Figure 7 shows the modification.

A new cathode follower was designed. There were difficulties involved in designing of the circuit. Some of the major trouble was the inherent high noise in the output, and a large C-3 ionosonde interference. Therefore, a 20-henry choke was used to attenuate random noise. Condensers are for C-3 RF bypasses. The circuit is shown in Figure 8.

Directional Photometer.

The electronic circuit of the directional photometer was originally designed by McIlwain of the State University of Iowa. The circuit was slightly modified for the Antarctic use. The modifications involve the replacement of 12AX7 with 12 AT7 and the removal of power circuit from the photometer turret. The preamp and the transistorized power supply were built in the photometer optical compartment in the original design. Yet the entire system stopped operation due to the low temperature (below 60° F). Therefore, only the photomultiplier tube was left in the optical compartment.

Further attention should be paid to the connecting wires. All the ordinary rubber insulation was utterly useless, since it

cracks and breaks. Special cold temperature wire must be used. There are at least three wires necessary to take the 1P21 output, i.e., photocathode, anode, and the 9th dynode. Such terminals were exposed under the snow. It was found that the snow accumulations on these terminals caused considerable difficulties. Various circuit parameters were changed due to this modification. The original circuit is shown in Figure 9. A logarithmic amplifier was used to cover a wide dynamic range. Figure 10 shows the calibration curve. Since photometers were used mainly to measure the time sequence of various events, we only noted the proper logarithmic behavior of the circuit from Figure 10. The effective aperture of the photometer is 0.0413 steradian. The entire photometer turret was mounted on the tripod base. Thus the photometer could be directed to any desired direction in the sky.

All Sky Photometer.

The function of the All Sky photometer is to monitor the all sky radiation in S-4 response [RCA tube handbook]. Therefore, the aperture is 2π steradian. The optical system is similar to that of the all sky camera, using 1.4 objective 25 mm [Elvey et al., 1957]. The circuit is analogous to that of the directional photometer. Figure 11 and Figure 12 show the schematic circuits,

which were designed and built by the author based on the directional and spectrograph photometers.

The optical system was elevated from the roof about eleven inches to avoid interference from the All Sky camera indicator lamps. Since the All Sky photometer is sensitive to any visible aurora in the sky, the output was connected to the 12AU7 cathode follower with a relay in place of the cathode resistance. An auroral alarm bell was thus activated by this relay. The circuit was designed and constructed by the author.

5.

VLF Equipment

A very low frequency receiving and recording system was developed at the Radioscience Laboratory of Stanford University. The band width of the receiver is 150 cps to 30 kc/s. In order to record the intensity of VLF emission continuously, a special clipper circuit was devised, which was designed by Morse of NBS and the author and built by the author. The system eliminates sferics of a short duration and records "hiss". Figure 13 shows the circuit diagram.

The R1 controls the phase of the clipped pulse. The R2 is the gain control, the R3 is the pulse height bias setting, and the

R4 is the position control for the Esterlein Angus recorder. Figure 14 shows a block diagram of the entire VLF system at the South Pole [Morozumi, 1961b].

6.

Magnetometer

A cathode ray tube 6462 was used to measure the magnetic field electrically. The electrical drift was rather large and no attempt was made to calibrate the system. However, the sensitivity was about 300 γ per inch.

The detector was placed about 300 feet from the science building to avoid interferences. The direct reading magnetometer of this kind is useful for the brief measurement of the magnetic field, whereas the standard photographic magnetometer requires processing before the measurement.

The circuit was originally designed by W. Hough of NBS, and modified by Morozumi for current use. Figure 15 shows the modified circuit diagram.

The detector could measure Z, H, or F, according to the orientation of the tube axis relative to the field vector.

III. SUMMARY OF THE DATA OBTAINED

A. Visual Program.

About 6,500 visual cards were obtained from April 16 to September 8, 1960. Also, 600 pages of extensive visual sketches of the aurora with simultaneous observations of VLF hiss were made on the MIT research notebooks. The sky condition was reported by the member of the USWB every hour.

B. All Sky Camera.

The All Sky Camera was in operation from April 16 to September 8, 1960. The 5577 interference filter was used to extend the operation to the end of the spring twilight. Five thousand feet of Tri-X film were obtained. All the contents were reviewed by the author and transferred to IBM punch cards by Mrs. DeLong of WDC-A.

C. 35-mm Color and B/W Aurora Photographs.

About 200 color pictures of the aurora were taken with Super Ektachrome. Tri-X was used to take about 1,000 black and white aurora photographs.

		Recorder Speed	
D.	Photometers.		
	1. Meridian Photometer	3/4 in. per hour	5 rolls each
	2. Directional Photometer	3/4 in. per hour	5 rolls each
	3. All Sky Photometer	3/4 in. per hour	4 rolls each
E.	Magnetogram.	3/4 in. per hour	7 rolls each
F.	VLF Recorder.	3/4 in. per hour	3 rolls each
G.	Cosmic Ray Monitor.	3/4 in. per hour	1 roll each
H.	Brush Recorder	1 mm per second	7 rolls each

I. All USCGS data and a part of NBS C-3 ionosonde data and Stan-VLF data were microfilmed for future analysis.

IV. DATA CODIFICATION AND REDUCTION

All aurora data, except spectrograph data, and other important geophysical parameters were tabulated in the manner discussed below and transferred to the IBM punch cards at the Cornell WDC-A.

The following information was immediately available from the IBM cards.

The auroral beginning, peak and ending time, measured by the All Sky photometer. All magnetic bays were listed in the same manner with their magnitude. Each disturbance was assigned a certain serial number from the beginning of the season. About 590 sets of disturbances were counted during the 1960 season. Then the entire sky was divided into 48 sectors to locate the auroral position exactly. This information was reduced from the All Sky camera data by using a movie editing machine. The visual data were also combined. Auroral forms were listed under eight major categories. Such categories were further divided into two or three sub-classes.

The brightness of the aurora was reduced from the All Sky Photometer data and the Visual Data. There are two types of brightness. One is the brightness of the All Sky relative to the

quiet night sky. Second is the brightness of the particular auroral form relative to the background.

The motions of the aurora were reduced from the visual data and the All Sky Camera film. Two kinds of motions were clearly differentiated. One is the motion of the aurora as a whole, second is the more complicated, rapid, local motion. Entire data reduction was done by the author.

Cloud data were provided from the USWB. Entire magnetic data, including K planetary and K south pole, were listed. The intensity of VLF hiss was recorded on magnetic tape and scaled aurally by Morse of NBS. A part of the audio spectrum was reviewed by an analyzer at Stanford University. In addition to the tape, VLF hiss intensity was recorded continuously, the quantitative information of which was listed. The C-3 ionosonde data for the types of E_s F_{min} and the total absorption was taken from the f-plot. In addition to the above information, daily average temperature, and the sun's and the moon's angles were recorded.

Such data are now being analyzed at the Cornell University and the State University of Iowa. Figure 16 shows a typical data sheet showing one day's summary. Seventy nine columns were used to transfer the above information to the punch card. Since it is impossible to analyze all of the above data, we selected a few items

of interest, namely, the correlation between VLF and aurora.

The following information is the key for decoding Figure 16

1. Universal time. All events are listed under the indicated time, e.g., 0100 included 0100 to 0159.
2. The beginning of the event in minutes. The number without square indicates magnetic activity. The number with square indicates auroral activity measured by the All Sky Photometer.
3. The peak time of the event.
4. The end of the event.
5. The display serial number, counted from the beginning of the 1960 aurora season.
6. The mode of auroral intensity distribution vs. time.
7. The location of the aurora, the sky divided into 48 sectors.
8. Form of the aurora in 17 classes.
9. Intensity of the aurora. 0 indicates the brightness of a form, v indicates the All Sky brightness relative to the quiet night air glow level.
10. Motion of the aurora in two categories.
11. Cloud number, name of the cloud.
12. USCGS magnetometer data.
13. Stanford VLF data.
14. VLF hiss peak time.
15. VLF hiss amplitude.
16. VLF hiss duration.

17. VLF chorus.

18. VLF whistler.

19. Universal time.

NB. The above column numbers are not analogous with the IBM punch card column numbers. We made cards on hourly basis. The following analysis is made, therefore, from 3432 cards.

V. ANALYSIS OF THE RESULTS

In the analysis of the data, an attempt was made to eliminate all possible interference. Thus the data were selected from the winter nights with relatively few clouds in the sky. The cloud observations were made by members of the USWB every hour. When the opaque coverage was less than seven-tenths, the data were considered to be valid. The solar depression angle was more than 11 degrees and the lunar elevation was less than 14 degrees south. Sixty-six per cent of June, July and August data met the above requirements, which was equivalent to 1425 cards. The data were coded and computed on the IBM 101 at Cornell WDC-A.

The results are tabulated in Tables I and II. K_{sp} is the average K index at the South Pole. F_m is the F layer minimum reflection frequency. Aurora has two columns. Aur-1 shows the average intensity. The method of computation is exactly the same as K_{sp}. The weight of each point is as follows: V 4, B 3, M 2, and F 1. /Kimball et al., 1957/ Aur-2 shows the percentage of all aurora presented in a given one hour period. We selected auroras of intensity of more than 1.5 in this computation. Without this limitation, it was difficult to see the diurnal change due to the frequent occurrence of auroras.

TABLE I

DIURNAL VARIATION OF VARIOUS EVENTS

U.T.	Ksp	Mc/s F_m	Aur.% 1	Aur.% 2	% HA,B	% RA,B	% r	% B	% VLF
0	3.76	1.42	1.03	33	43	33	14	2	22
1	3.70	1.27	1.02	33	40	27	16	0	33
2	3.70	1.98	1.15	54	48	30	7	4	26
3	3.54	1.28	.98	29	20	15	20	0	14
4	3.50	1.35	.69	25	15	15	10	3	5
5	3.39	1.21	.63	27	17	12	7	2	2
6	3.33	1.34	.59	19	9	14	9	0	5
7	3.30	1.35	.55	15	5	10	18	0	0
8	3.35	1.55	.55	28	10	8	15	3	8
9	3.59	1.38	.57	39	5	15	24	2	0
10	3.70	1.49	.69	41	2	20	32	12	2
11	3.68	1.57	.68	45	3	18	40	5	3
12	3.80	1.86	.66	55	5	25	45	8	6
13	3.79	2.05	.61	37	3	16	32	16	5
14	3.83	2.37	.52	18	3	15	23	5	10
15	2.75	1.81	.41	18	0	8	28	8	5
16	2.83	1.57	.35	15	0	10	15	7	0
17	2.75	1.45	.46	5	2	5	24	0	12

TABLE I CONTINUED

U.T.	Ksp	Mc/s F_m	Aur. % 1	2	% HA,B	% RA,B	% r	% B	% VLF
18	2.37	1.26	.67	23	20	10	15	0	26
19	2.36	1.26	.72	27	27	20	22	0	22
20	2.38	1.23	.83	15	26	13	23	0	19
21	2.80	1.15	.73	15	30	10	20	0	26
22	2.80	1.24	.96	22	37	5	7	0	29
23	2.87	1.41	.93	21	45	15	10	0	41

Aur. 1 : average intensity v = 4
2 : intensity 1.5

r : ray

B : non deviative absorption

$$\% = \frac{\text{\# of events}}{\text{\# of cards per given hour}}$$

TABLE II

VARIOUS EVENTS AS A FUNCTION OF K

K_{SP}	Mc/s F_m	% Aur.	% HA,B	% RA,B	% r	% B	% VLF
1	1.27	3	3	1	7	2	1
2	1.25	1	13	8	12	0	9
3	1.43	20	20	13	21	1	14
4	1.65	42	15	25	28	4	14
5	1.64	52	25	25	20	11	13
6	1.85	54	43	23	23	11	43
7	2.94	57	43	21	14	0	21

It is clear from the tables that the intensity distribution and occurrence distribution of aurora are quite different. Percentage occurrence of 1200 U.T. for example, is about the same as that of 0200 U.T. However, the intensity of the aurora is almost doubled at 0200 U.T. From this example, we see immediately that the midnight displays are mostly consisted of brighter auroras than the noon auroras. However, an occurrence of midnight auroras is less frequent than noon auroras (Figure 17A). HA,B and RA,B are homogeneous arcs and bands, short ray arc and bands respectively. The r stands for long rays and coronas. The B is the ionospheric total absorption. And lastly the VLF hiss occurrence is shown. In order to see the results from the different points of view, Table II was constructed.

Then we plotted Figure 17 from Table I. In the figure, we see the diurnal variation of the following:

a Aur-1, solid line. Aur-2, dotted line.
b Magnetic K index.
c Homogeneous arcs and bands.
d VLF hiss.
e Long rays and coronas.
f Ionospheric absorption of letter B /Atlas of Ionogram, 1957/ measured by C-3 ionosonde.

The abscissa of the graph indicates the universal time. The magnetic midnight is 04:40 U.T.

The percentage occurrence was computed by taking the ratio of the number of the events to the total number of cards at each one-hour interval (Table I). Since there are 1425 cards, about 60 cards correspond to one hour's data.

There are two aurora peaks in the diurnal variation curve (Figure 17A). Figure 18 shows typical 24 hour records of auroral light by (a) zenith and (b) all-sky photometer. No filters were used in either case. Note that these data well represent the diurnal curve of Figure 17A. The peak at around U.T. midnight or about three hours before the magnetic midnight was mostly due to HA, HB type of aurora which usually went through a typical auroral display sequence.

Note the statistical agreement between the diurnal variation of VLF hiss and HA,B type of aurora, which suggests that the above phenomena is locally observed from the geographical point of view.

Considering the physical significance of such a correlation /Ellis, 1957; Gallet, 1959/, a close examination of these statistical results were made by one-to-one correlation study.

There are two classifications of arc and band type auroras. The first class is the display of arcs and bands without prominent development. The other type is arcs and bands which were followed

by break-ups. However, in either case, hiss was associated with the display in more than 50 per cent of the cases when bright HA, HB aurora and intense hiss were selected (Figure 17).

Figure 19 shows a general relationship between the magnetic VLF and aurora data. Figures 20, 21 and 22 are corresponding All Sky camera data for Figure 19. In reference to Figures 19 and 20, the spectrum of the auroral hiss compared with the quiet time spectrum are shown in Figure 23. Such auroral hiss noise intensity was recorded when arc and band type of aurora of the first class appeared, Figure 24. To illustrate the second class, All Sky photometer white light data was superimposed on the VLF data to see the time sequence between the two events, Figure 25. Note a sharp VLF hiss peak (about two minutes duration) in the beginning of the auroral development. The same event was magnified by a fast speed recorder, Figure 26. The corresponding All Sky camera data, Figure 27, showed that the VLF hiss peak time coincided with the HA, HB stage of the auroral development. However, when aurora broke up into an active form and arrived at the zenith, VLF hiss intensity decreased a great deal in spite of an increase in the auroral total light intensity. The same associations were shown elsewhere [Morozumi, 1961b, Morozumi, 1962]. In Figure 27 the magnetic north is left and west is bottom of the frame. A glow in the direction of

the magnetic west is twilight. Disregard the exposure of 2244 U.T., which is a long exposure in the automatic data cycle to check faint auroras.

When the second class of auroral display and the VLF hiss was studied, hiss peak clearly preceded the auroral light peak in 71 per cent of the cases. The average time lead was 8.5 minutes. The cessation of the signal may be due to the ionspheric absorption /L. H. Martin et al., 1960/ or radiation pattern of the source.

The duration of the South Pole hiss is extremely short compared with that of the low latitude hiss; average duration was 11 minutes.

The secondary peak of aurora diurnal occurrence at around U.T. noon, or a few hours before the magnetic noon, was dominated by series of sporadic long rays and corona, Figure 17E.

The characteristic of such aurora is its low luminous intensity and an association with large ionospheric effects. Usually the F minimum frequency increase is quite prominent, (Table I). Most of the ionospheric nondeviative absorption occurs at this time, Figure 17F. The aurora in between these two peaks are mixtures of both types. Therefore, we may observe arc and band type of aurora and long rays at the same time with VLF hiss. It seems that when unusual departure of magnetic K planetary index from the average

value takes place, the regular diurnal variation pattern discussed above may be disturbed a great deal and non-hiss type of aurora may appear at around U.T. midnight, when hiss-type of aurora usually dominates and vice versa. Close examination of the F plot showed that 62 per cent midnight (magnetic midnight 4:40 U.T.) aurorae without hiss were attributed to the ray type. Figures 28 and 29 show an example of ray type auroras. Such aurora was characterized by the appearance of unusually high F minimum frequency in C-3 ionosonde data.

The following is a typical qualitative description of the aurora event with hiss from the visual log. In the beginning, a faint trace of hiss starts to appear on the recorder. A weak hiss may last for awhile intermittently. The aurora at this time is either glow or faint HA on the northern magnetic horizon. As the hiss intensity becomes higher, homogeneous arc changes to intense bands. The motion of the aurora is mostly lateral. Then very short fine ray-like structures start to appear on the auroral bands. These short ray-like structures move very rapidly. The intensity of the VLF hiss seems associated with the brightness of the aurora and its motion. The noise seems loud when the brighter end of the band changes its shape. Extremely intense noise is often associated with auroras with pinkish lower borders. Within five to fifteen

minutes, all the forms break up into rays and draperies, advancing southward very rapidly. After the break-ups, VLF hiss usually stops. The fact is in good agreement with the result from the qualitative analysis.

Once the aurora attains the maximum activity, the display decays by leaving patchy luminous surfaces in the sky. Sometimes, however, another noise burst is observed, which again is associated with the aurora arc and bands. The period of recurrence was less than two hours, average interval of about 70 minutes.

To summarize, we found close correlation between VLF hiss and the auroral arcs and bands at the south geographical pole. The VLF hiss does not seem to be characteristic of all auroras, but has a special association with auroral arcs and bands. Since auroral arcs and bands were usually observed in the beginning of the display, the detailed investigation of VLF hiss may help the study of the cause of the noise itself and also the cause of the primary excitation mechanism of a certain type of auroras.

In the next chapter we review briefly the possible mechanism for production of radio noises and associated phenomena.

VI. THEORIES OF RADIO WAVE EMISSION FROM PLASMA AND ASSOCIATED PHENOMENA

Consider the energy conservation between photons and kinetic energy of the particle. The radio wave emission or photons will be produced at the expense of the kinetic energy of the particle. The reverse is the acceleration of the particles at the expense of photon energy.

First we review the radio wave emission mechanisms. They are

1. Plasma oscillation
2. Bremsstrahlung
3. Cerenkov radiation
4. Cyclotron emission
5. Synchrotron radiation
6. Traveling wave tube

Mechanisms 1 through 3 do not require external magnetic field. However, 4 and 5 are familiar phenomena found in particle accelerator, i.e. magnetic bremsstrahlung. Microscopically, particles are losing their kinetic energy by Cerenkov process to the photons in theory 6.

We consider briefly the reverse phenomena which may be of interest, namely, the acceleration of particles at the expense of

photon's energy. In the high energy region, Compton scattering is a good example. The other possibility is Landau damping.

1. Plasma oscillation:

The mechanism of charged particle oscillations to account for the anomalous scattering was detected and discussed by Tonks and Longmuir, [1929].

Consider a bounded plasma region under the condition described by Tonks et al., where the negative and positive particles are distributed evenly. The resultant space charge is zero. Then the electrons, due to their light mass, will oscillate about their equilibrium position if the neutrality of the charge is distributed in any manner.

Suppose the electron displacement from the initial position is ζ and the boundary planes to be X_1 and X_2, the limit in the change of the electron concentration Δn is

$$\Delta n = -n \frac{\partial \zeta}{\partial X}$$

The resultant space charge creates an electron field which can be calculated from Poisson's equation

$$\nabla \cdot E = -\frac{e\,\Delta n}{\epsilon_0} \longrightarrow \frac{\partial E}{\partial X} = \frac{ne}{\epsilon_0} \frac{\partial \zeta}{\partial X}$$

Since the space charge field is zero when the displacement is zero

$$E = \frac{ne}{\epsilon_0}\,\zeta$$

This field which acts on the electrons arises solely from their displacement and is a longitudinal field in the direction of the displacement.

Applying the force law,

$$m_e\ddot{\zeta} = -Ee = -\frac{ne^2}{\epsilon_0}\zeta \qquad \therefore\ \omega_p^2 = \frac{ne^2}{m_e\epsilon_0}$$

Thus the frequency of the plasma electron oscillation is a function of the electron concentration [Field, 1956; Condon, 1958] and

$$\nu \approx 8,980\sqrt{n}$$

From the rocket observations [Friedman, 1959], n may be

$\sim 10^6/cm^3$ (200 km)

then

$$\nu \approx 10 \text{ mc/s.}$$

From the emission mechanism [Chamberlain, 1961], only electrons are considered at this height.

Some of the observational facts, such as the motion of the

intense auroral structure and hiss noise, etc., are attractive to the plasma oscillation theory. However, in general, quantitative interpretation of plasma oscillation is difficult /Bekefi and Brown, 1961/.

2. Bremsstrahlung:

Balloon and rocket flights detected X rays of 10 to 100 kev, which is attributed to the Bremsstrahlung from the primary auroral electrons /Van Allen, 1957; O'Brien, 1962/.

Classical calculation of bremsstrahlung for electron-ion encounters are satisfactory in radio frequencies also /Bekefi and Brown, 1961/.

The frequency of emission is

$$\omega = \frac{m}{2\hbar}\left(V_i^2 - V_f^2\right)$$

where V_i, V_f are the initial and the final velocity of the particles.

Radio emission may arise from fast secondary electrons, /Chamberlain, 1961/.

Further possibilities of bremsstrahlung will be discussed under cyclotron and synchrotron radiation.

3. Cerenkov radiation:

The existence of Cerenkov radiation is well established at optical frequencies, when a fast charged particle travels through

an optical medium whose refractive index is greater than the ratio of the velocity of the light to the particle velocity, i.e.

$$\eta > \frac{c}{v} \quad , \quad \cos\theta = \frac{c}{\eta v} \tag{1}$$

where θ is the angle between one field and the electron's velocity vector [Chamberlain, 1961]. The radio wave emission from the Cerenkov radiation was discussed by Marshall and Ellis [Ellis, 1957b; Marshall, 1956].

This radiation can be predicted as a solution of Maxwell's equation for a charged particle in uniform rectilinear motion through a medium in which the velocity of the electromagnetic radiation is less than the particle velocity. The radiation is not a function of the mass of particle [Mather, 1951; Panovsky and Phillips, 1955].

Complex refractive index of magneto-ionic medium is given by Appleton's equation

$$\eta^2 = 1 - \frac{X}{1 - iZ - \frac{\frac{1}{2}Y_T^2}{1 - X - iZ} \pm \left[\frac{1}{4}\frac{Y_T^4}{(1 - X - iZ)^2} + Y_L^2\right]^{1/2}} \tag{2}$$

where

$$\omega_p^2 = \frac{ne^2}{m_e \epsilon_o}$$

$$\omega_H = \frac{\mu_o H_o e}{m_e} \cos\phi$$

$$\omega_T = \frac{\mu_o H_o e}{m_e} \sin\phi$$

$$X = \frac{\omega_p^2}{\omega^2} \qquad Y = \frac{\omega_H}{\omega} \qquad Y_L = \frac{\omega_L}{\omega} \qquad Y_T = \frac{\omega_T}{\omega}$$

$$Z = \frac{\nu}{\omega}$$

$$\tan\phi = \frac{H_T}{H_L}$$

/Ratcliff, 1959, p. 19/.

However η could be simplified to

$$\eta^2 = 1 + \frac{\omega_p^2}{\omega(\omega_H - \omega)} \qquad (3)$$

for the longitudinal extraordinary mode [Helliwell and Morgan, 1959] combining equations 1 and 3, we obtain

$$\omega = \frac{\omega_H}{2}\left[1 \pm \left\{1 - \left(2\frac{\omega_p}{\omega_H}\frac{V\cos\theta}{c}\right)^2\right\}^{1/2}\right]$$

If $Vw_p/2$ c is 2 Kc/s [Gallet, 1959], w will be .425 and 9.42 Kc/s when $w_h/2$ is 9.84 Kc/s.

The radiation pattern of Cerenkov emission is maximum along $\bar{B}$ [Mather, 1951].

4. Cyclotron emission:

The cyclotron emission is a noncollisional mechanism such that the mean free path must be long enough for a particle to make a complete turn between collisions under the magnetic field. Non-relativistic expression of the frequency is

$$\omega_h = \frac{Be}{m}$$

In contrast to bremsstrahlung, cyclotron emission is anisotropic. In general, it is elliptically polarized [Bekefi and Brown, 1961].

The radiation pattern is maximum along B, i.e., B's maximum, where S is Poynting vector. When the angle between B and S is 90°, the wave not only changes its amplitude but also changes

its original frequency due to the existence of electrons in the path.

We may be able to explain a long duration of low latitude hiss by this transverse mode of hiss propagation as particles drift along longitude. Of course, the frequency of the received signal is greatly modified in such cases. If the optical depth is more than unity, the radiation will be that of a Black body.

Cyclotron emission is one of the possibilities for the VLF hiss emission. Although an individual frequency is discrete, the resultant frequency could be a continuum. This is apparent from the expression of frequency, which is a function of B. Proton cyclotron emission frequency in the earth field is calculated by Aarons [1960], which is in the order of 800 cps or lower. Electron cyclotron frequency varies from 1.5 MC to few Kc/s.

5. Synchrotron radiation:

When the velocity of the particle approaches that of light, the radiation from the cyclotron mechanism changes its pattern [Van Allen, 1962]. The frequency of the emission must be corrected with the relativistic mass. Most of the radiation energy resides in the higher harmonics of gyrofrequency. The relativistic doppler correction must also be made for the duration of one pulse for the computation of Fourier integral [Van Allen, 1962].

The radiation pattern is maximum in the plane of gyration [Panofsky and Phillips, 1955].

The expression for the maximum frequency is

$$\nu = 10.7 \; B \epsilon^2 \quad Mc/s$$

where B is in gauss and ϵ in Mev [Bekefi and Brown, 1961].

The total intensity of radiation over all frequency is

$P = 6.1 \times 10^{-22} B^2 \epsilon^2$ watts per electron [Bekefi et al., 1961].

6. Traveling Wave Tube Theory:

The essential physics of the traveling wave tube is in its interaction of high energy plasma with the electromagnetic wave [Pierce, 1950]. The condition for the interaction is that the propagating electromagnetic wave has a longitudinal component of electric field along the phase direction of the propagation. The initial electromagnetic energy may come from the thermal noise in the exosphere or any minute electromagnetic perturbation which is amplified as they propagate. Calculations for whistler propagation show that at relatively low frequencies the phase velocity can be as low as c/100 in some part of the atmosphere [Gallet, 1959]. For those conditions, the combination of the exospheric plasma and the magnetic field plays the role of very effective slow-wave structure [Gallet, 1959].

In the above case, the condition for the amplification is

$v_p = V$ (1) where v_p is the phase velocity of the electromagnetic wave; V is the velocity of the incoming plasma.

The local refractive index is

$$\eta = \left[1 + \frac{\omega_p^2}{\omega\omega_H - \omega^2} \right]^{1/2} \tag{2}$$

and $$v_p = \frac{c}{\eta} . \tag{3}$$

Combining (1) and (3) and solving for w gives

$$\omega = \frac{\omega_H}{2} \left[1 \pm \left\{ 1 - \left(2 \frac{\omega_p}{\omega_H} \frac{V}{C} \frac{1}{\sqrt{1-\beta^2}} \right)^2 \right\}^{1/2} \right]. \tag{4}$$

Since the value of the expression

$$\frac{1}{\sqrt{1-\beta^2}} \approx 1 \tag{5}$$

(4) can be simplified with great accuracy to

$$\omega = \frac{\omega_H}{2} \left[1 \pm \left\{ 1 - \left(2 \frac{\omega_p}{\omega_H} \frac{V}{C} \right)^2 \right\}^{1/2} \right]. \tag{6}$$

This equation is the basic expression of the theory. Thus the frequency emitted by the process is the function of the velocity of the plasma, the earth's field, and the density of the particles.

7. Landau damping:

The reverse of the traveling wave tube theory is Landau damping, which is a mechanism whereby electrons whose thermal velocity is near the phase velocity of a plasma wave can abstract energy from it [Bekefi and Brown, 1961].

8. Propagation of the signal in the magneto-ionic medium:

Stimulated transitions are more probable at radio than at optical frequencies [Matsushima, 1962].

The expression for the absorbing transition is $B_{12}\ I_V$ where B_{12} is the Einstein coefficient. The $B_{21}\ I_V$ is induced by the radiation field at the same time. Therefore, two Einstein coefficients are related by

$$B_{12} = \frac{G_2}{G_1} B_{21}$$ where G is the statistical weight.

Combining the Boltzman formula

$$\frac{N_2}{N_1} = \frac{G_2}{G_1} e^{-h\nu/kT}$$

so that

$$\frac{G_1 N_2}{G_2 N_1} = e^{-h\nu/kT}$$

Hence the net absorption coefficient, α_ν', becomes

$$\alpha_\nu' = \alpha_\nu(1 - e^{-h\nu/kT}) \qquad T<0,\ T>0$$

In the optical region $e^{-h\nu/kT}$ will be neglected. However, in the radio range, the contribution from the $e^{-h\nu/kT}$ term must be considered. Therefore, the radiation induced emission becomes very large. Under such conditions, the medium will behave like an amplifier to the incident radiation, or negative absorption phenomena [Twiss, 1958; Gordon et al., 1955].

This mechanism was applied to the laboratory experiment. The MASER, microwave amplification by stimulated emission of radiation is the device which utilizes the above principle [Gordon et al., 1955; Smith, 1961]. The theory is applied to the production of radio waves from aurora by Twiss [Twiss, 1958].

Various theories were reviewed. If we assume the excitation mechanism of the plasma oscillation in the ionosphere [Chamberlain, 1961], the computed frequency of emission is too high for the VLF hiss.

Cerenkov radiation is a good possibility. If this is the

case, the radiation should appear to come from the zenith of the observer. Electron cyclotron mechanism could emit frequencies below 1.5 Mc/s. This radiation also appears to come from the magnetic zenith of the observer. However, in case of a synchrotron mechanism the radiation is a minimum in the direction of B.

In any case, the traveling-wave-tube type amplification may be taking place in the exosphere. For further study we need a quantitative measurement of the power emitted from the source and accurate measurement of the spectral distribution.

VII. DISCUSSION AND CONCLUSION

The aurora is believed to be the visual excitation of the gases in the upper atmosphere by energetic incoming particles. It is estimated that auroral particles take twenty to thirty hours to travel from the sun to the earth [Gartlein, et al., 1962]. Combining Meinel's observation [Gerson, et al., 1954] and the absorption of Ca^+ ion [Mitra, 1952], the particle velocity must be around 2-3000 km/s.

Recent observations showed evidence of dumping of high energy electrons of 40 to 100 kev at an altitude of 1000 km at high latitude [O'Brien, 1962].

In order to account for the large difference of the velocity of the particles in the above two measurements, the energy exchange between electromagnetic waves and the kinetic energy of the particles was considered. Although we were unable to advance plausible theory on this mechanism, we were able to arrive at few characteristics of VLF by the following reasoning. Since the auroral observations were limited in the visible range (see Figure 5), any observation which has a diurnal occurrence ratio proportional to the auroral occurrence must be limited in the same geographical range.

Judging from the close agreement of VLF hiss and the auroral diurnal variation curve, we think that VLF hiss may be propagated in a quasi-longitudinal mode.

The strong diurnal recurrence suggests the solar origin of the observed phenomena.

Therefore, the most favorable interpretation of the observations may be the combination of the cyclotron and Cerenkov theories with the Helliwell-Gallet theory. Considering the large range of possible emission regions, the frequency of the emission may very well vary between a few kc/c to mc/s.

Further, we conclude that those particles which are injected at around magnetic mid-night are capable of producing an intense hiss and the band type of aurora. There must be a strong spatial concentration of the ionospheric current in or above these band type of aurora. A careful analysis of the magnetogram and the all sky camera data showed such relationships (see Figure 30). In the figure, at the time a, the edge of the aurora is about to pass the zenith. The aurora is overhead at the time b. The last edge of the auroral band passed through the zenith at the time c. We will study this interesting topic at some other time. On the other hand, those particles which are injected at around magnetic noon (roughly corresponds to local noon at low

latitude) are capable of producing large ionospheric effects, such as non-deviative absorption, etc. Probably the occurrence of such aurora decreases as the latitude decreases not only due to the sunlight but also due to the low magnetic rigidity of the particles.

Suppose this is the case: we should observe more ray type aurora and less arc type aurora inside the aurora zone. Therefore, we may receive less VLF hiss there.

Since the noon aurorae are caused by the direct solar wind, the location of the rays are sporadic, whereas the midnight aurorae are well focused by the earth's field.

The above model also explains the shift of aurora toward the magnetic pole at magnetic noon. Therefore, aurora must have an antisymmetric zone which may rotate with the sun.

The general conclusion arrived at on the comparison between two auroral maxima from this study is shown in Table III.

Now, in order to explain the HA,B type of auroras and VLF hiss diurnal curve (Figure 17), we assumed a curved path of the solar particles. One of the most striking points is the sudden decrease of HA,B type of auroras and VLF hiss occurrence after magnetic midnight. The diurnal curve showed a peak at about three hours before magnetic midnight. Since the earth rotates about 15 degrees per hour, three hours corresponds to 45 degrees east of

TABLE III

	MIDNIGHT Peak	NOON Peak
Auroral Occurrence	Less frequent	Frequent
Auroral Brightness	Bright	Less bright
Duration of Display	Long 1 ~ 2 hours	Sporadic
Auroral Forms	Arcs and bands with frequent break-ups	Long rays and corona
Auroral Location	Mostly northern horizon, large displays advance toward south	Mostly zenith
VLF	Strong hiss	Chorus
Ionsphere	Blackout only with bright auroras	Blackout or high F minimum
Geomagnetism	Large deflection only with bright auroras	Frequent perturbations of small amplitude

the magnetic meridian. If our interpretation is correct, the possibility of solar particle penetration increases gradually until the apparent location of the sun is 45 degrees east of the magnetic meridian and decreases rapidly. There should be very little or no chance for solar particle penetration after magnetic midnight.

From this study, we see clearly that VLF technique is a powerful new method of observing the solar corpuscular radiation. Different from the auroras, the VLF technique is independent of local interferences, such as clouds, moonlight, and twilight. However, one large disadvantage is the existence of the ionosphere, which is optically transparent but opaque to radio waves of certain wave lengths.

Thus it is desirable to carry out VLF experimentation from space vehicles above the ionosphere. Such measurement will provide the true spectrum and exact location of the VLF source in space, which will undoubtedly give more information, not only on the emission mechanism but also the relationship between Van Allen particles and the aurora.

From a theoretical point of view, understanding of the VLF phenomena requires a vast amount of knowledge on the magneto-ionic

medium. The energy exchange between the electromagnetic wave or low energy photons and the kinetic energy of the particles, for example, is indeed an interesting subject.

REFERENCES

Aarons, J., and M. Henissart, "Low-Frequency Noise in the Range 0.5-20 Cycles Per Second", Nature 172, 682-683 (1953).

Aarons, Jules, "Low Frequency Electromagnetic Radiation 10-900 Cycles Per Second", J. Geophys. Research 61, 647-661 (1956).

Aarons, J., A. Egeland, and G. Gustufsson, "Audio-Frequency Electromagnetic Radiation in the Auroral Zone", J. Geophys. Research 65, 2749-2758 (1960).

Allcock, McK. G., "A Study of the Audio-Frequency Phenomenon Known as 'Dawn Chorus'", Australian J. Phys. 10, 286-298 (1957).

Bekefi, G., and S. C. Brown, "Emission of Radio-Frequency Waves from Plasmas", Am. J. Phys. 29, 404-428 (1961).

Burton, E. T., and E. M. Boardman, "Audio-Frequency Atmospherics", Proc. Inst. Radio Engrs. 21, 1476-1494 (1933).

Chamberlain, J. W., Physics of the Aurora and Airglow, Academic Press, New York and London, 1961, p. 704.

Clark, E. S., "Diurnal Variation of Antarctic Aurora", Unpublished M.S. Thesis, Department of Physics, Cornell University, February 1, 1961.

Condon, E. W., and H. Odishaw (ed.), Hand Book of Physics, McGraw-Hill Book Co., Inc., New York, Toronto, London, 1958.

Ellis, G. R., and G. Reber, "Cosmic Radio-Frequency Radiation Near One Mc/s", J. Geophys. Research 61, 1-10 (1956).

REFERENCES (continued)

Ellis, G. R., "Cosmic Radio-Noise Intensities Below 10 Mc/s", J. Geophys. Research 62, 229-234 (1957a).

Ellis, G. R., "Low-Frequency Radio Emission from Aurorae", JATP 10, 302-306 (1957b).

Ellis, R. G., "Simultaneous Occurrence of Sub-Visual Aurorae and Radio Noise Bursts on 4.6 Kc/s", Nature 183, 1618 (1959).

Ellis, G. R., "Directional Observations of 5 Kc/s Radiation from the Earth's Outer Atmosphere", J. Geophys. Research 65, 839-843 (1960a).

Ellis, G. R., "Geomagnetic Disturbances and 5 Kc/s Electromagnetic Radiation", J. Geophys. Research 65, 1705-1710 (1960b).

Ellis, G. R., "Spaced Observations of Low-Frequency Radiation", J. Geophys. Research 66, 19-23 (1961).

Elvey, C. T., and W. Stoffregen, "Auroral Photograph by All-Sky Camera", Ann. IGY 5, Part II, 117-151 (1957).

Field, G. B., "Radiation by Plasma Oscillations", Astrophys. J. 124, 555-570 (1956).

Friedman, H., "Rocket Observations of the Ionosphere", Proc. Inst. Radio Engrs. 47, 272-280 (1959).

Gallet, R., "The Very Low-Frequency Emission from the Earth's Ekosphere", Proc. Inst. Radio Engrs. 47, 211-231 (1959).

Gartlein, C. W., et al., "IGY General Report Number 12", Nov., 1960.

REFERENCES (continued)

Gartlein, C. W., R. C. Bless, D. S. Kimball, and G. Sprague, "Aurora, Magnetic Bays and Protons", J. Geophys. Research 64, 949-953 (1959).

Gartlein, C. W., and D. S. Kimball, "Visual Aurora Observation and Reporting for Observers in the United States of America during the I. G. Y., 1957/1958", Cornell University, Feb. 23, 1957.

Gartlein, C. W., and G. Sprague, "The Origin and Morphology of Auroras", Second Annual Report for N. S. F. Contract G-12439, Cornell 7405, January, 1962.

Gerson, N. C., T. J. Keneshea, and R. J. Donaldson, Jr. (ed.), Proceedings of the Conference on Auroral Physics, GRD AFCRC, 41-59, July, 1954.

Gordon, J. P., H. J. Zeiger, and C. H. Townes, "The Maser -- New Type of Microwave Amplifier, Frequency Standard, and Spectrometer", Phys. Rev. 99, 1264-1274 (1955).

Heppner, J. P., "A Study of Relationships between the Aurora Borealis and the Geomagnetic Disturbances Caused by Electric Currents in the Ionosphere", Ph.D. Thesis, California Institute of Technology, Pasadena, 1954.

Helliwell and Morgan, "Atmospheric Whistlers", Proc. Inst. Radio Engrs. 47, 200-208 (1959).

Helliwell, R. A., and D. L. Carpenter, "Results from the IGY/IGC 59 Synoptic Program", Trans. Am. Geophys. Union 43, No. 1, March, 1962a.

REFERENCES (continued)

Helliwell, R. A., Letter, 7 May 1962b.

Kern, J. W., and E. H. Vestine, "Theory of Auroral Morphology", J. Geophys. Research 66, 713-724 (1961).

Marshall, L., "Production of the Sun's Non-Thermal Radio Emission by Cerenkov Radiation", Astrophys. J. 124, 469-475 (1956).

Martin, L. H., R. A. Helliwell, and K. R. Marks, "Association between Aurora and Very Low-Frequency Hiss Observed at Byrd Station, Antarctica", Nature 187, 751-753 (1960).

Mather, R. L., "Cerenkov Radiation from Protons and the Measurement of Proton Velocity and Kinetic Energy", Phys. Rev. 84, 181-190 (1951).

Matsushima, S., "A Note Prepared for the Radio Astronomy 1961-1962, Second Semester", State University of Iowa, Department of Physics and Astronomy (Textbook, Shklovsky, see Van Allen).

Menzel, D. H., and W. W. Salisbury, "Audio-Frequency Radio Wave from the Sun", Nature 161, 91 (1948).

Mitra, S. K., The Upper Atmosphere, The Asiatic Society, Calcutta, India, 1952.

Morozumi, H., "Association between VLF Hiss and Auroral Arcs Observed at South Pole", Research Paper Presented at VLF-ELF Seminar at Stanford University, August 24, 1961a.

REFERENCES (continued)

Morozumi, H., "South Pole 1960 Aurora Air Glow Program", A Report to USRP, NSF Arctic Institute of North America, Sept. 2, 1961b.

Morozumi, H. M., "Association between VLF Hiss and Auroral Arcs and Bands", Technical Paper, Arctic Institute of North America, 1962.

O'Brien, B. J., "Direct Observations of Dumping of Electrons at 1000-Km Altitude and High Latitudes", J. Geophys. Research 67, 1227-1233 (1962).

Ondoh, T., "On the Origin of VLF Noise in the Earth's Exosphere", J. Geomagnetism and Geoelectricity 7, 77-83 (1961).

Panofsky, W. K. H., and M. Phillips, Classical Electricity and Magnetism, Addison-Wesley Publishing Co., Inc., Cambridge 42, Mass., 1955.

Pierce, J. R., Traveling Wave Tube, D. Van Nostrand Co., Inc., Toronto, New York, London, 1950.

Potter, R. K., "Analysis of Audio Frequency Atmospherics", Proc. Inst. Radio Engrs. 39, 1067-1069 (1951).

Radioscience Laboratory, Whistlers and VLF Emissions, 1959.

Ratcliff, J. A., The Magneto-Ionic Theory and Its Application to The Ionosphere, Cambridge at the University Press, 1959, p. 19.

RCA Tube Handbook, Vol. 3-4.

REFERENCES (continued)

Shain, C. A., and C. S. Higgins, "Observation of Cosmic Noise at 9.15 Mc/s", Australian J. Phys. 7, 460-470 (1954).

Shklovsky, I. S., Cosmic Radio Waves, Harvard University Press, Cambridge, Mass., 1960.

Smith, R. A., "Amplification through Stimulated Emission -- The Maser", British J. of Applied Physics 12, 197-206 (1961).

Stanford University, VLF-ELF Seminar at Stanford University, August 24, 1961.

Stormer, C., The Polar Aurora, Oxford at the Clarendon Press, 1955.

Tonks, L., and I. Langmuir, "Oscillations in Ionized Gases", Phys. Rev. 33, 195-210 (1929).

Twiss, R. Q., "Radiation Transfer and the Possibility of Negative Absorption in Radio Astronomy", Australian J. Phys. 11, 564-579 (1958).

Van Allen, J. A., "Direct Detection of Auroral Radiation with Rocket Equipment", Proc. of the National Academy of Science, 43, No. 1, 57-62, Jan., 1957.

Van Allen, J. A., "Dynamics, Composition and Origin of the Geomagnetically-Trapped Corpuscular Radiation", SUI Research Report 61-19, Aug., 1961.

Van Allen, J. A., Class Note for Radio Astronomy Given 1961-62, Second Semester, 1962 (Textbook Shklovsky, Cosmic Radio Waves, Harvard University Press, Cambridge, Mass., 1960).

REFERENCES (continued)

Watts, J. M., "An Observation of Audio-Frequency Electromagnetic Noise during a Period of Solar Disturbance", J. Geophys. Research 62, 199-206 (1957).

Willis, H. F., "Audio-Frequency Magnetic Fluctuations", Nature 161, 887 (1948).

Wright, J. W., and R. W. Knecht (ed.), "Atlas of Ionograms", CRPL, Boulder, Colo., 1957.

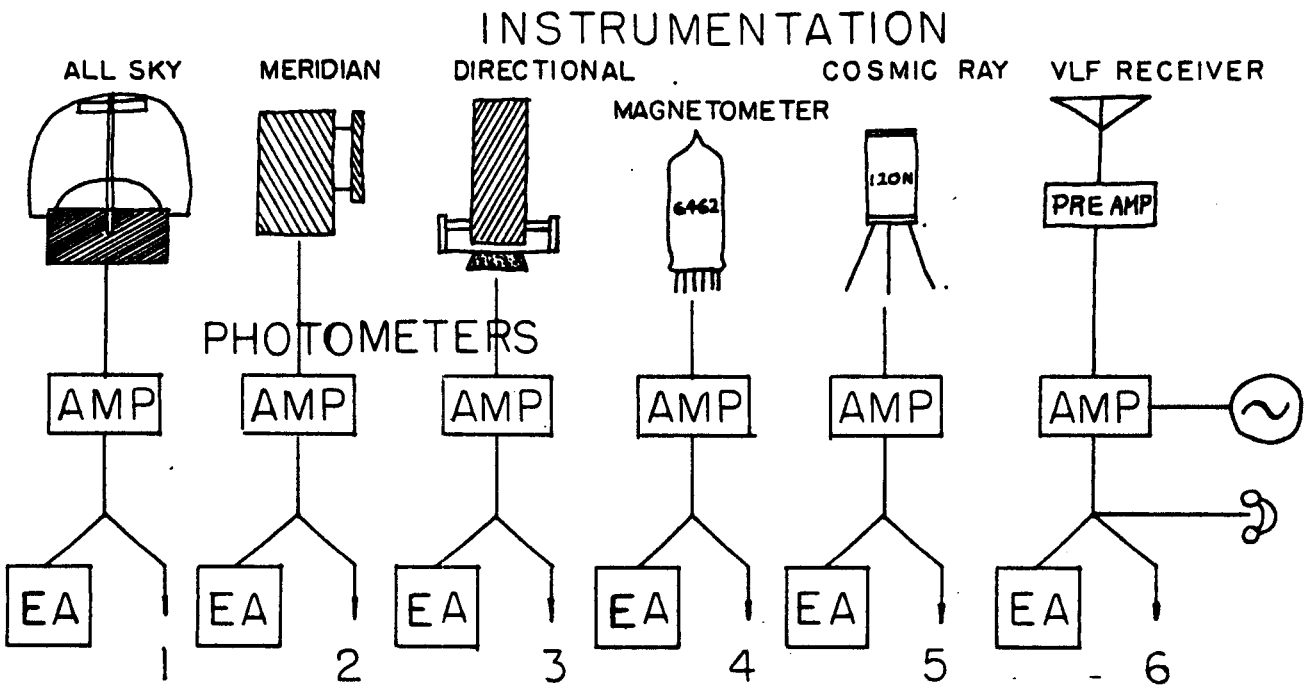

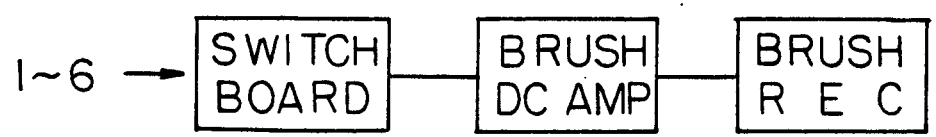

RECORDER SPEED EA : 3/4 IN/HR BRUSH : 1 MM / SEC FIG. 1

1. ALL SKY CAMERA
2. HATCH
3. VISUAL DOME
4. DIRECTIONAL PHOTOMETER
5. ALL SKY PHOTOMETER
6. SPECTROGRAPH

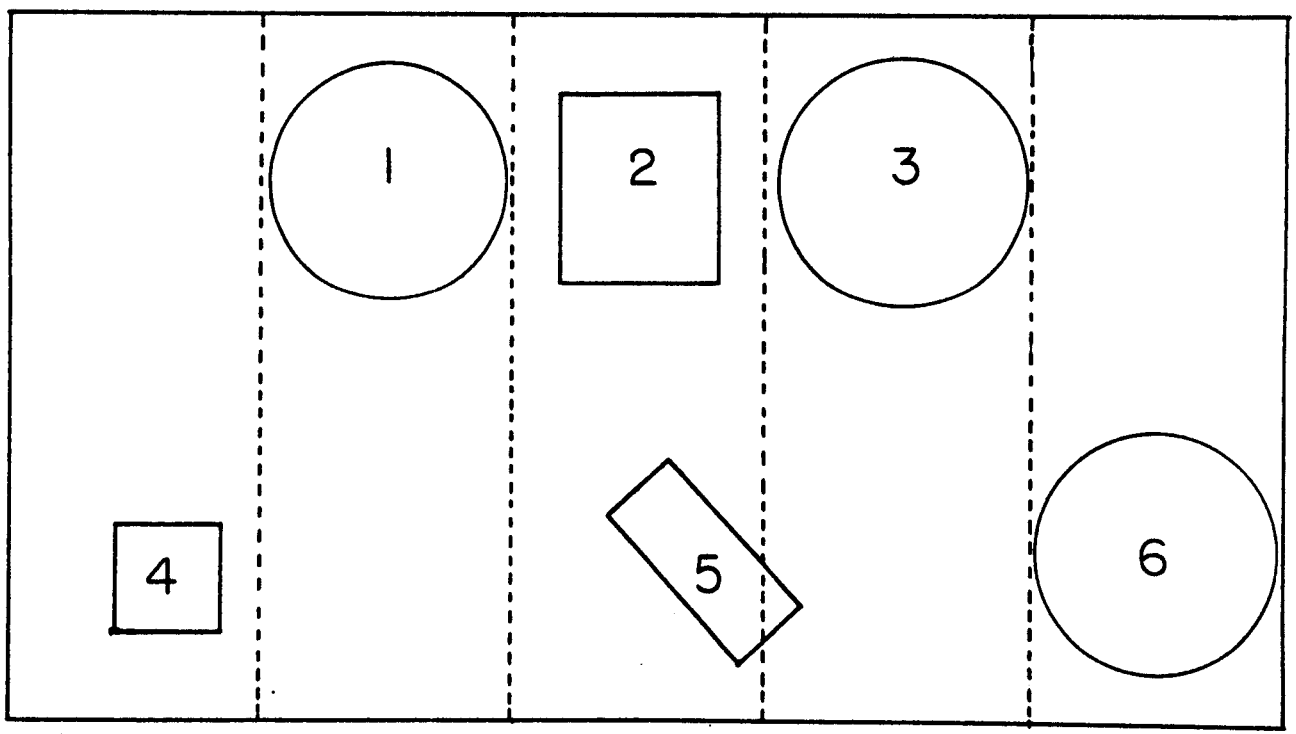

FIG. 2

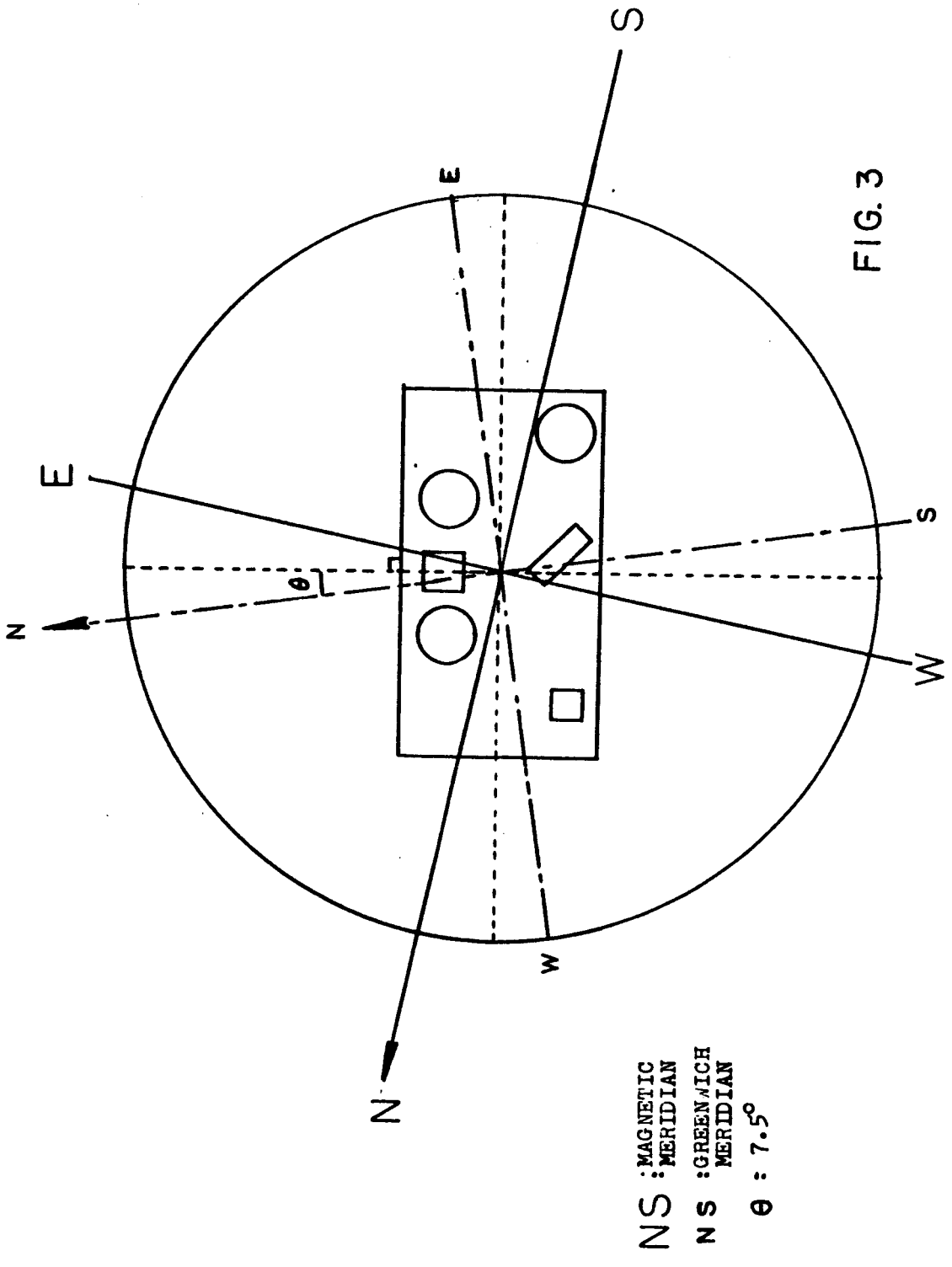

FIG. 3

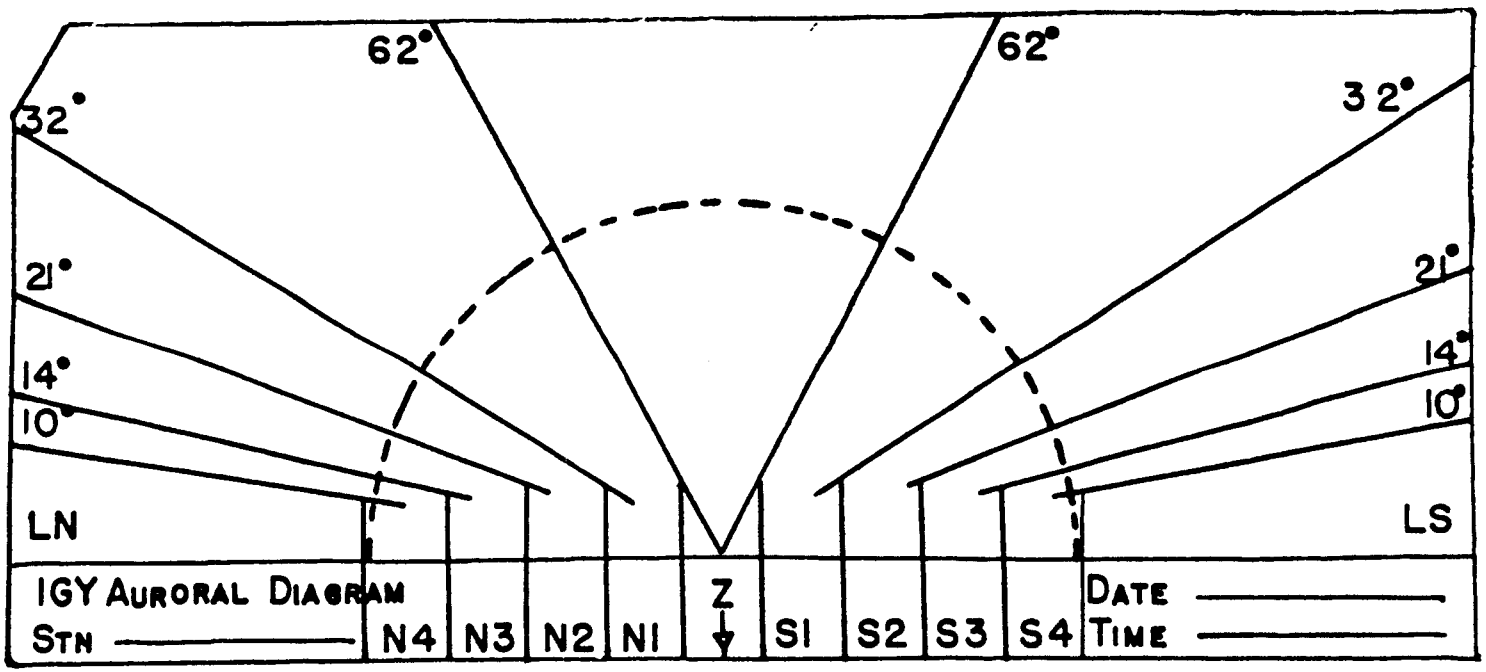
62°
62°
32°
32°
21°
21°
14°
14°
10°
10°
LN
LS
IGY AURORAL DIAGRAM
STN
N4
N3
N2
N1
Z
S1
S2
S3
S4
DATE
TIME

Figure 4

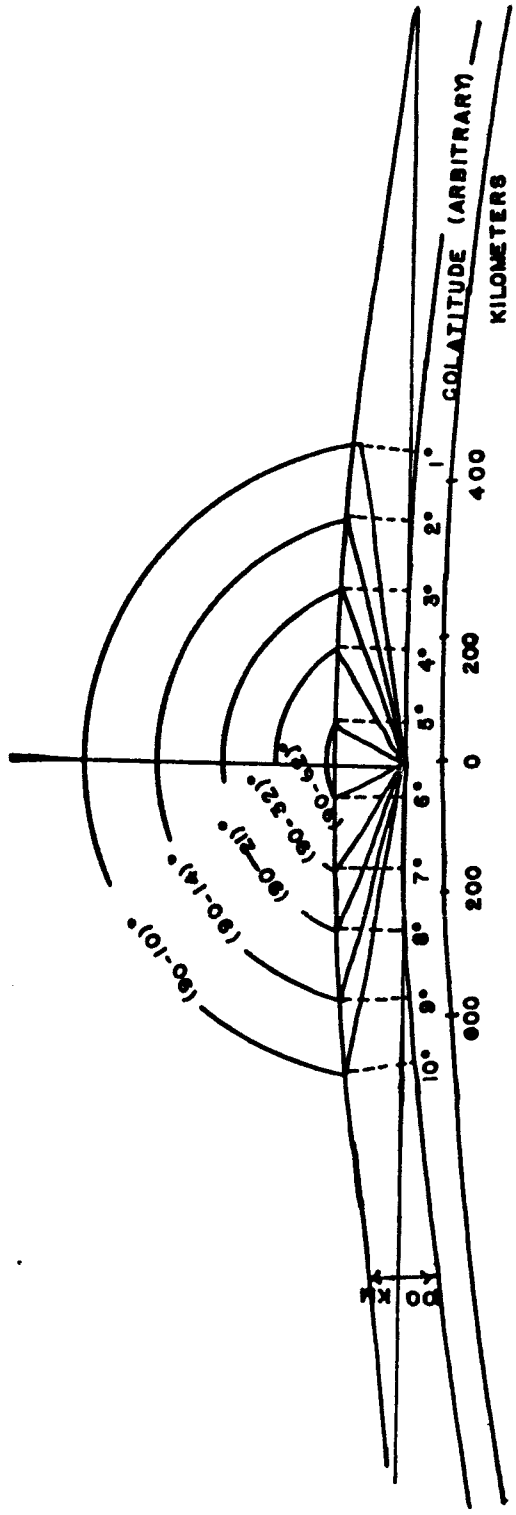
COLATITUDE (ARBITRARY)
KILOMETERS
1°
2°
3°
4°
5°
6°
7°
8°
9°
10°
400
200
0
200
600
(90-01)
(90-04)
(90-12)
(90-32)
(90-64)

Figure 5

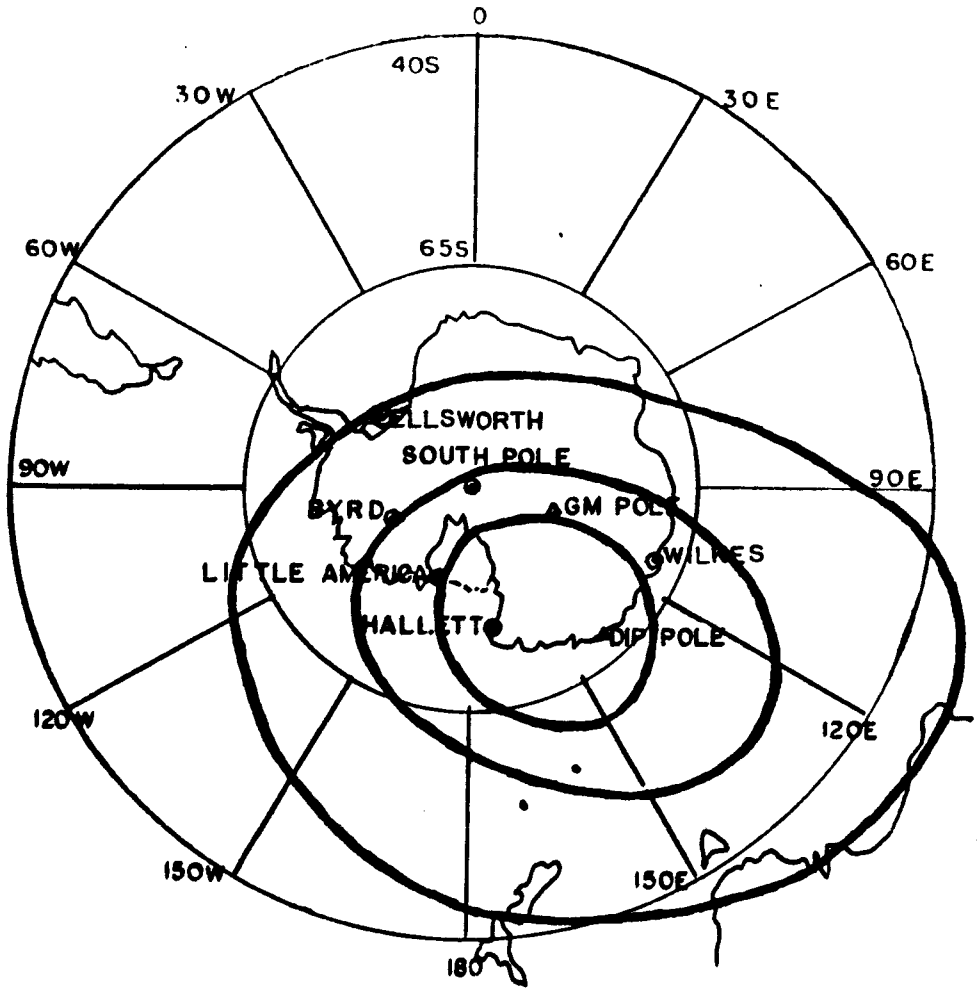
0
40S
30W
30E
60W
65S
60E
ELLSWORTH
SOUTH POLE
90W
90E
BYRD
GM POLE
WILKES
LITTLE AMERICA
HALLETT
DIP POLE
120W
120E
150W
150E
180

Figure 6

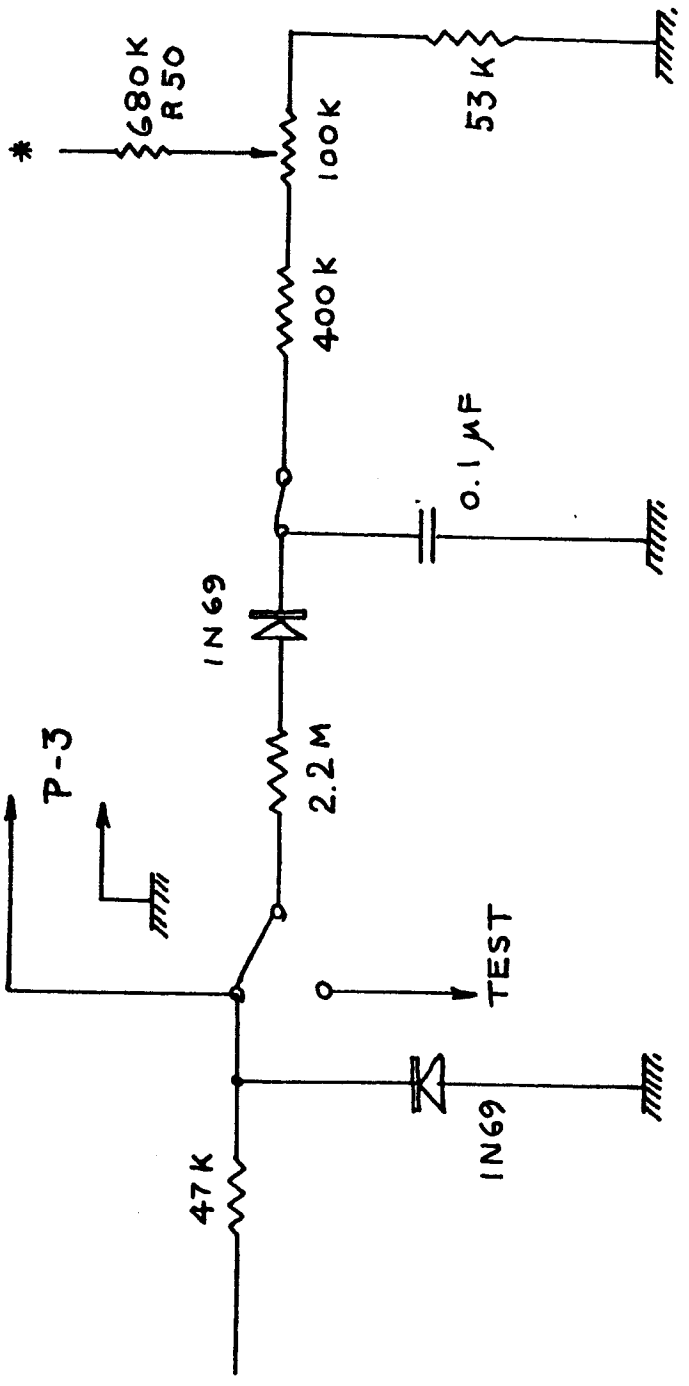
680K
R50
100K
53K
400K
0.1 μF
IN69
2.2M
P-3
TEST
IN69
47K
* TO PIN No 2 OF K2-W

FIG. 7

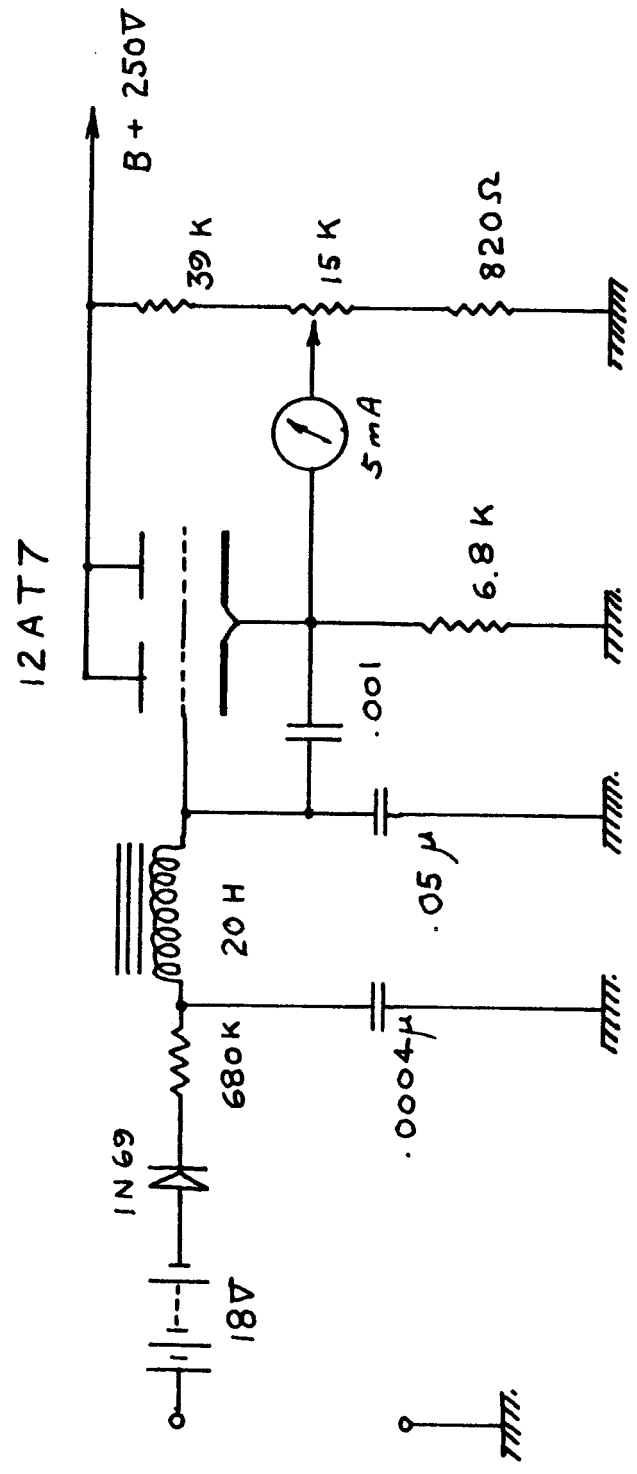
B + 250V
39 K
15 K
820Ω
5mA
12AT7
6.8 K
.001
.05 μ
20 H
680K
.0004μ
1N69
18V

FIG. 8

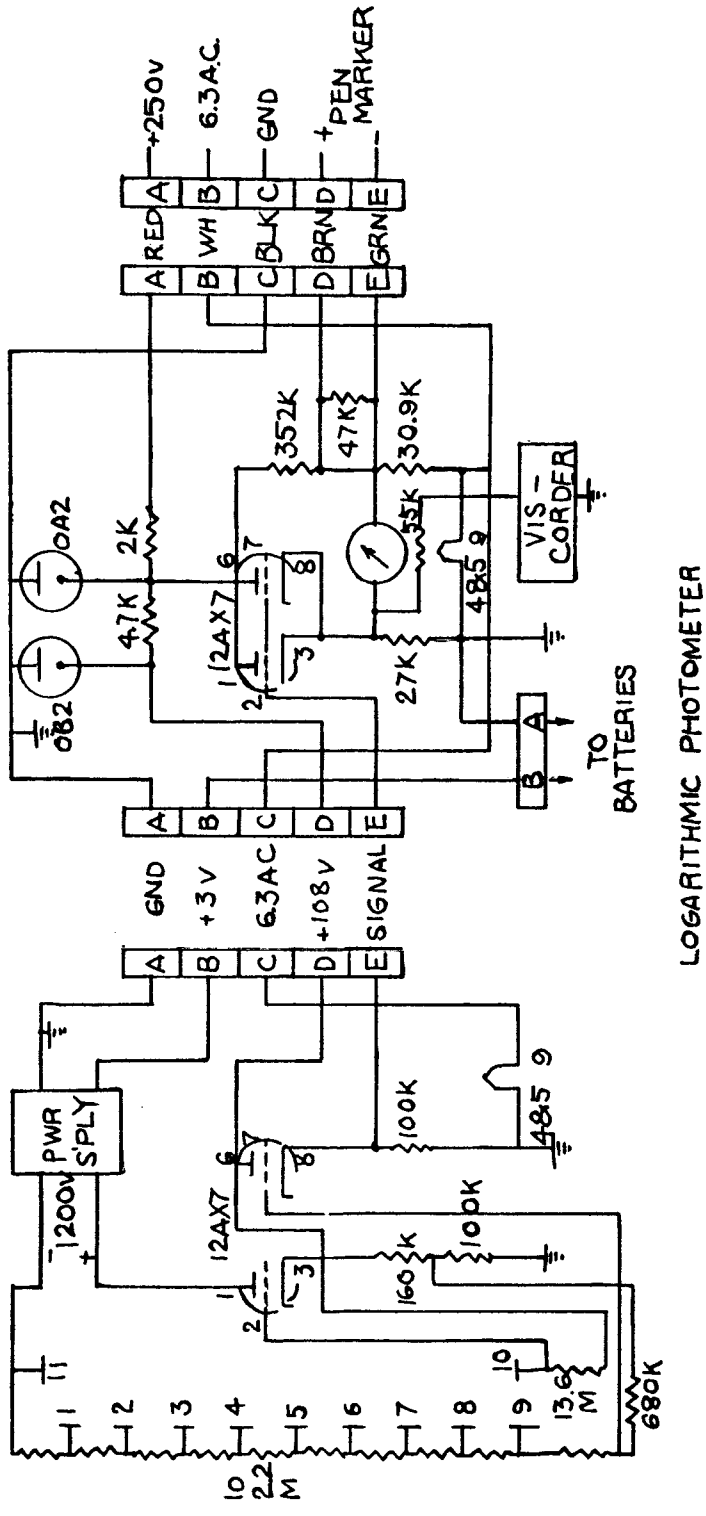

LOGARITHMIC PHOTOMETER

FIG. 9

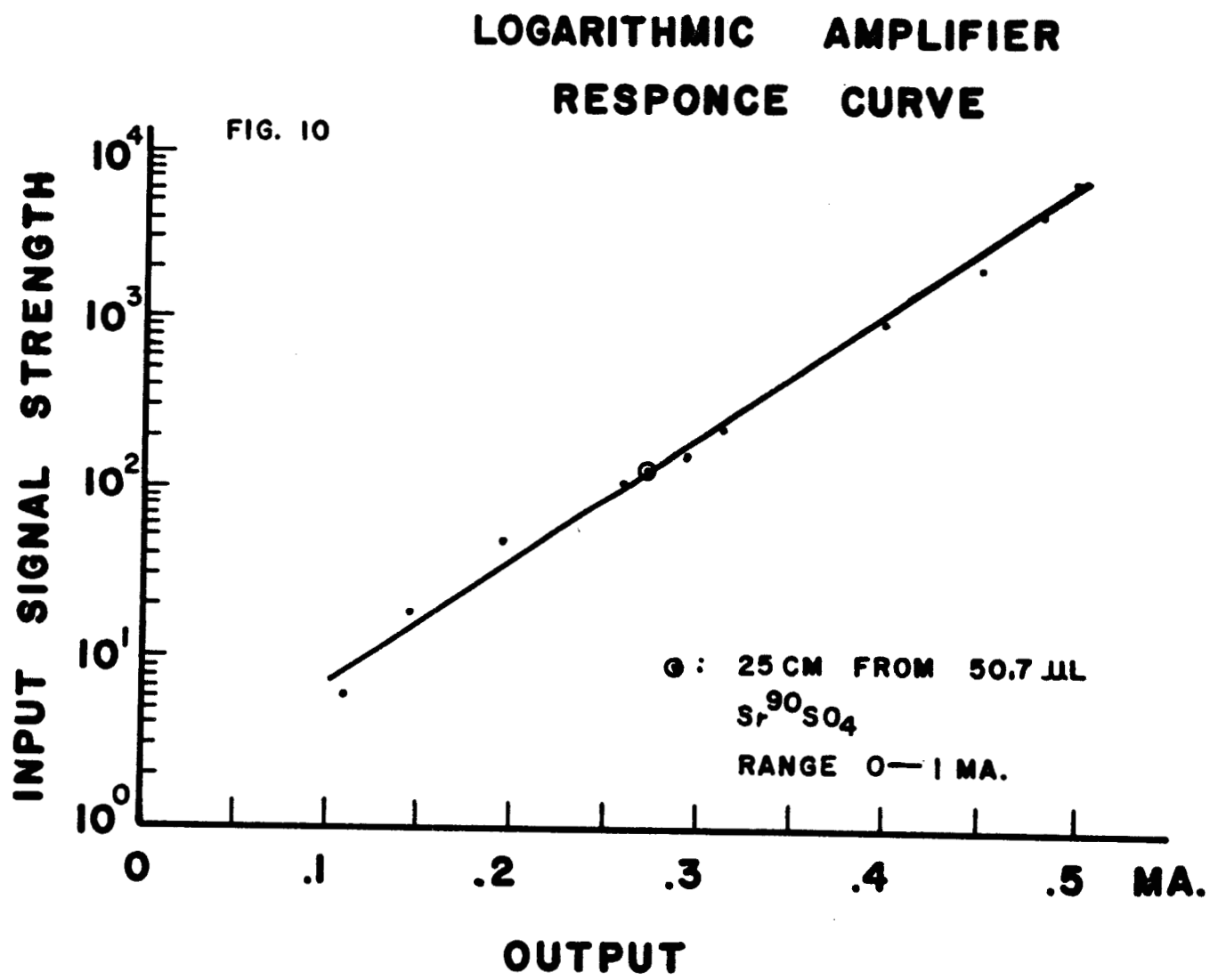
LOGARITHMIC AMPLIFIER
RESPONCE CURVE
FIG. 10
INPUT SIGNAL STRENGTH
10^4
10^3
10^2
10^1
10^0
0
.1
.2
.3
.4
.5 MA.
OUTPUT
⊙ : 25 CM FROM 50.7 µL
$Sr^{90}SO_4$
RANGE 0—1 MA.

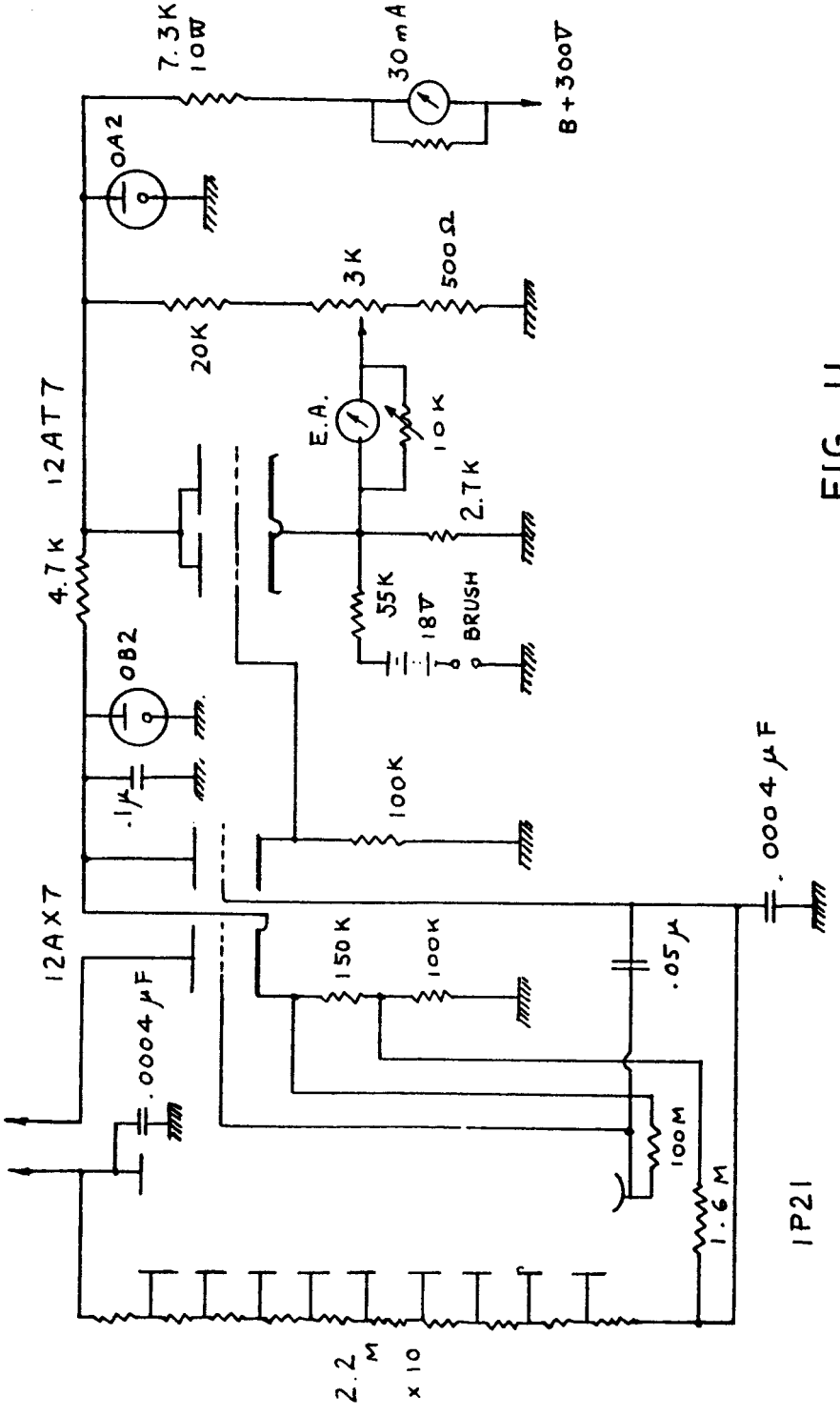
7.3K 10W
30mA
B+300V
0A2
3K
500Ω
20K
E.A.
10K
2.7K
12AT7
4.7K
55K
18V
BRUSH
0B2
.1μ
100K
.0004 μF
12AX7
150K
100K
.05μ
100M
1.6M
1P21
2.2 M
x10

FIG. 11

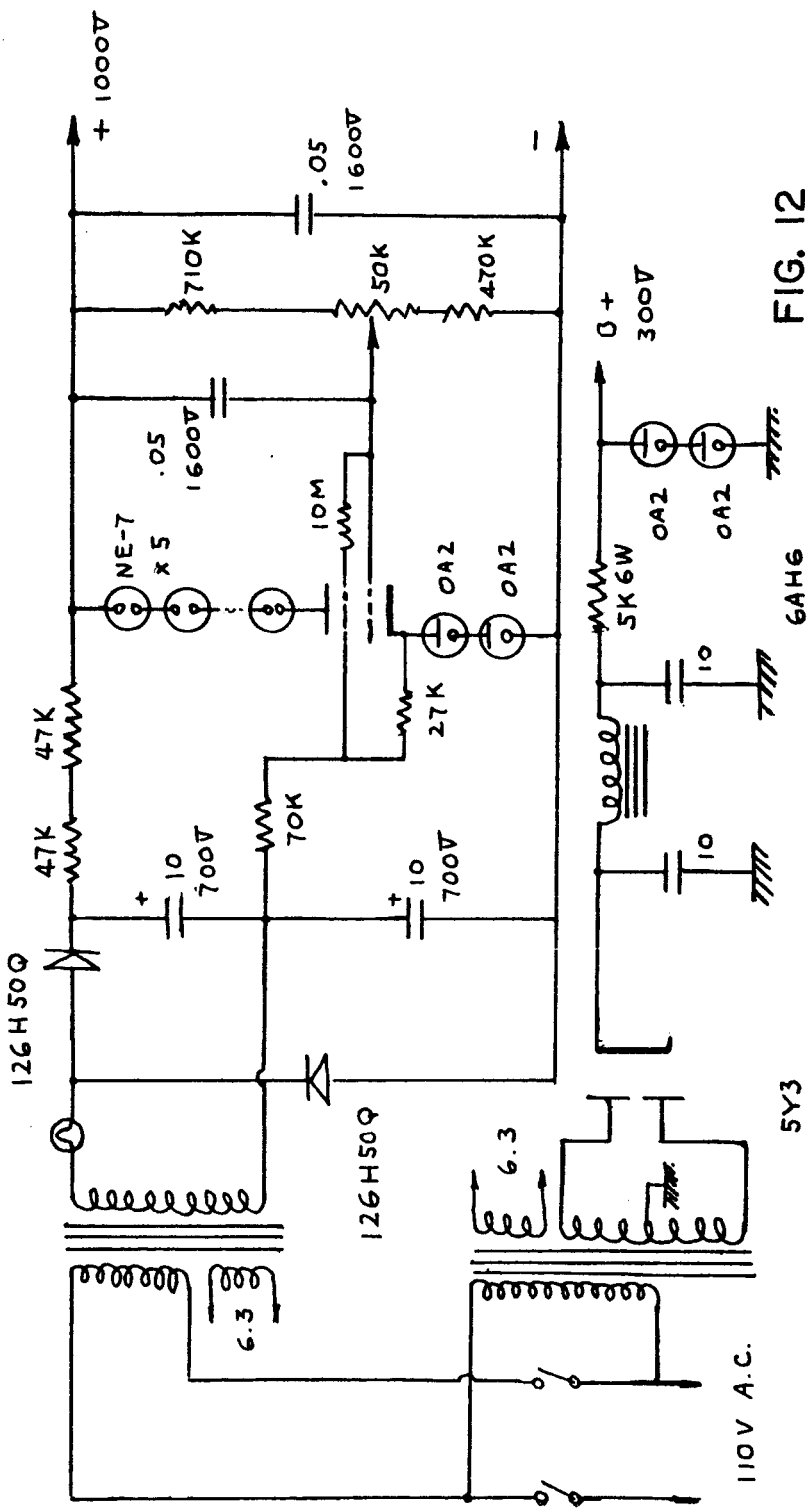
+ 1000V
.05
1600V
710K
50K
470K
0 +
300V
.05
1600V
10M
NE-7
x 5
0A2
0A2
0A2
0A2
5K 6W
6AH6
47K
47K
27K
10
700V
70K
10
700V
10
10
126H50Q
126H50Q
6.3
6.3
5Y3
110 V A.C.

FIG. 12

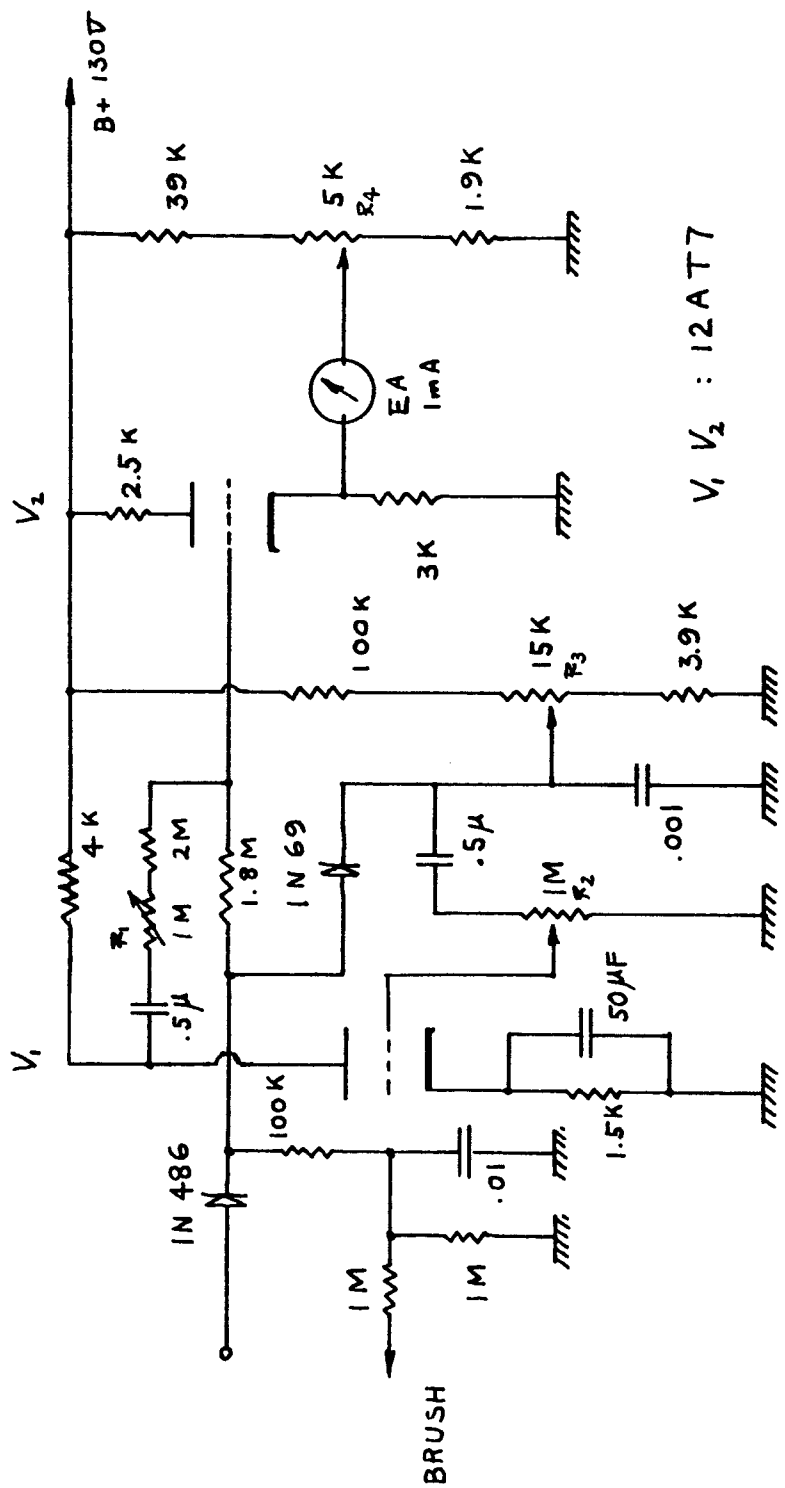
B+ 1300
39 K
5 K
R4
1.9 K
EA
1mA
3K
2.5 K
V2
100 K
15 K
R3
3.9 K
4 K
2M
1M
R1
.5μ
1.8M
1N69
.5μ
.001
1M
R2
50μF
V1
100 K
1.5K
1N 486
.01
1M
1M
BRUSH
V1 V2 : 12AT7

FIG. 13

VLF RECEIVING SYSTEM

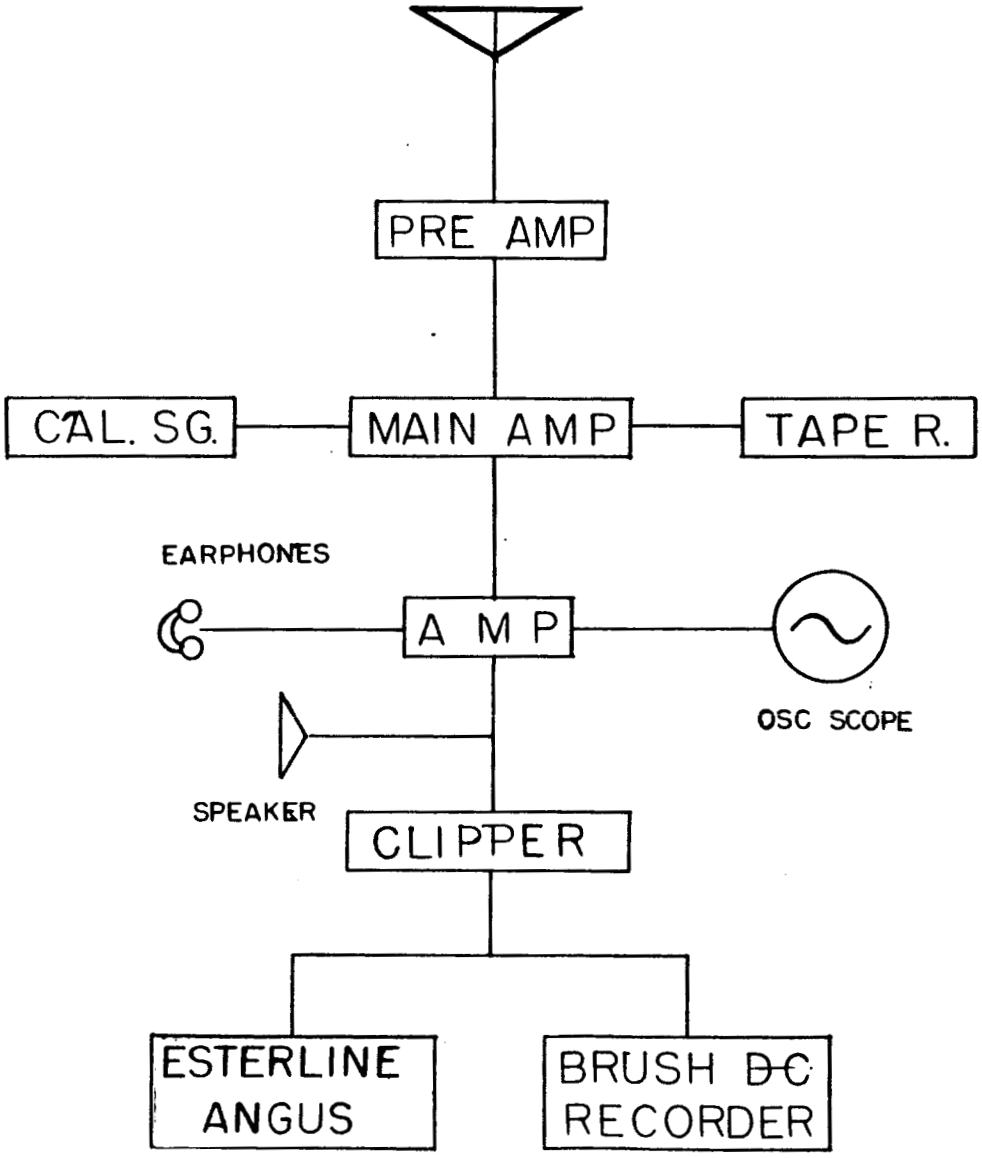

FIG. 14

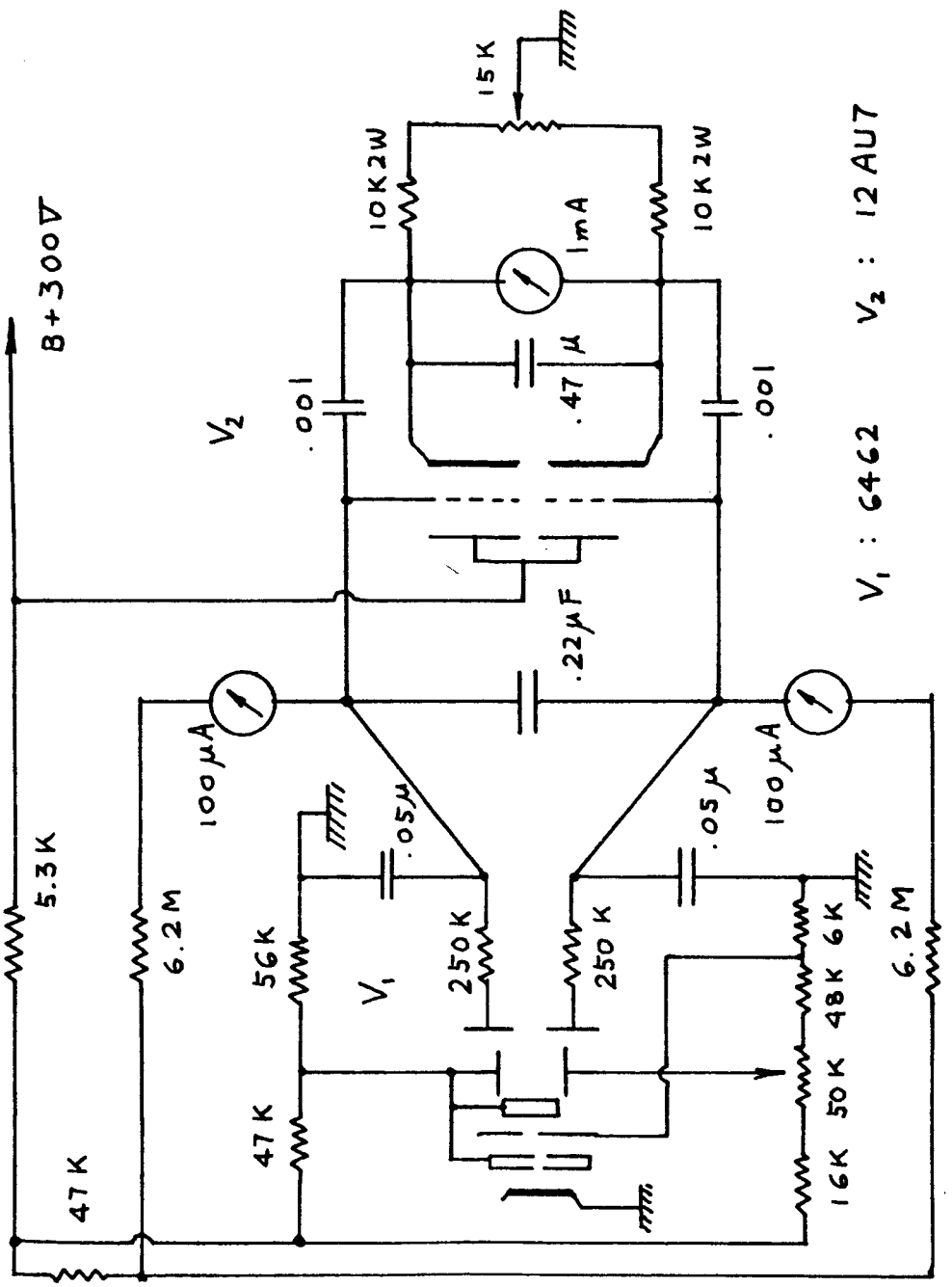
B+300V
15K
10K 2W
10K 2W
1mA
.47 μ
.001
.001
V2
.22μF
100μA
100μA
.05μ
.05μ
5.3K
6.2M
56K
250K
250K
6.2M
V1
47K
48K
6K
50K
16K
47K
V1 : 6462
V2 : 12AU7

FIG. 15

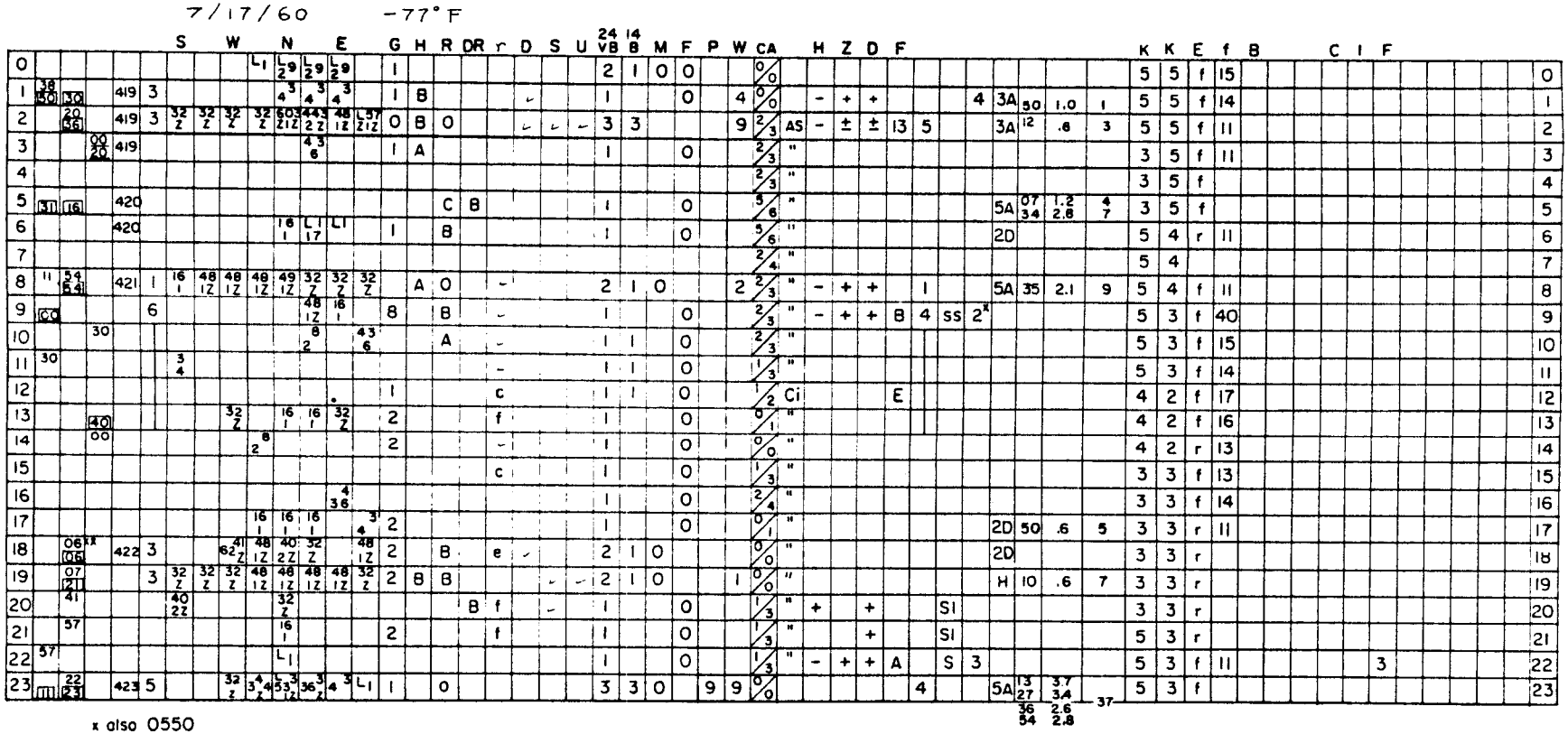

x also 0550

xx see original scaled at tΔH peak

Figure 16

DIURNAL VARIATION OF VARIOUS EVENTS

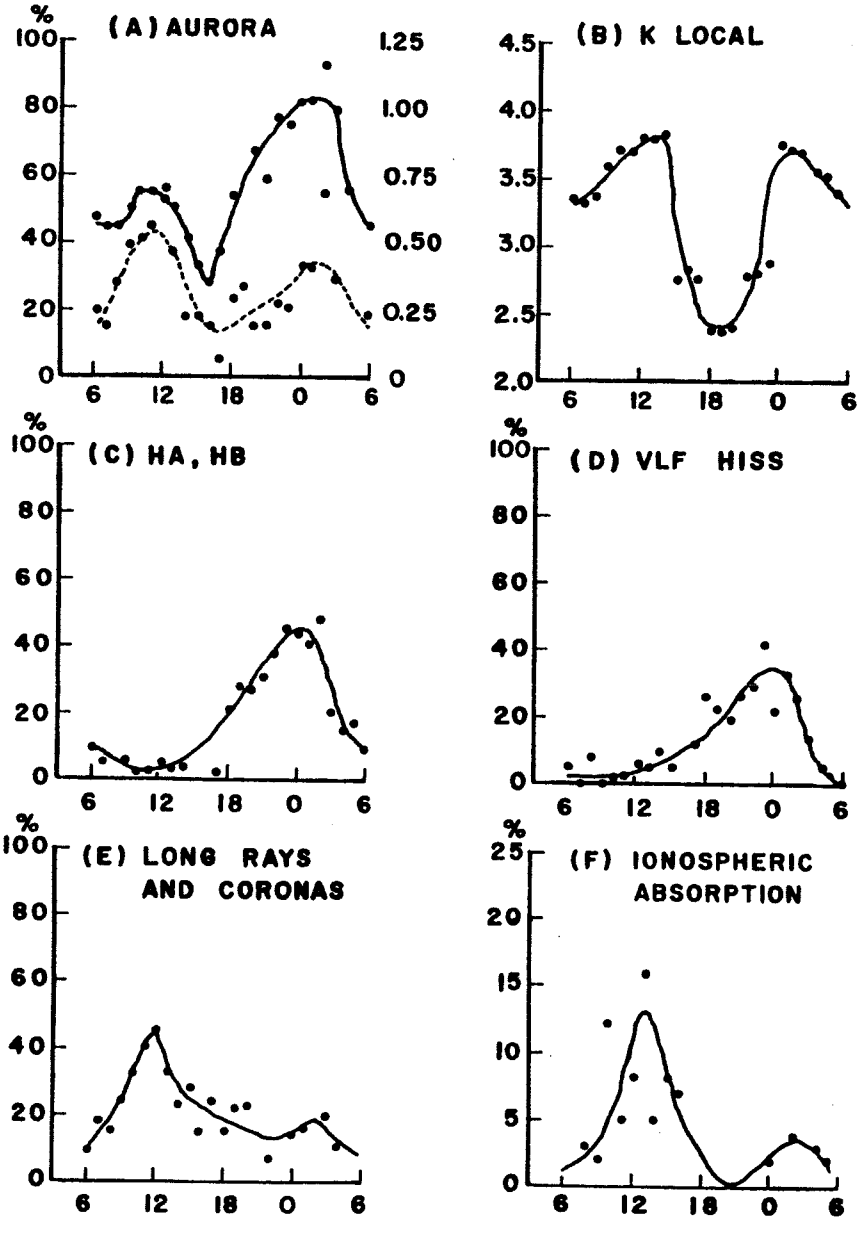

Figure 17

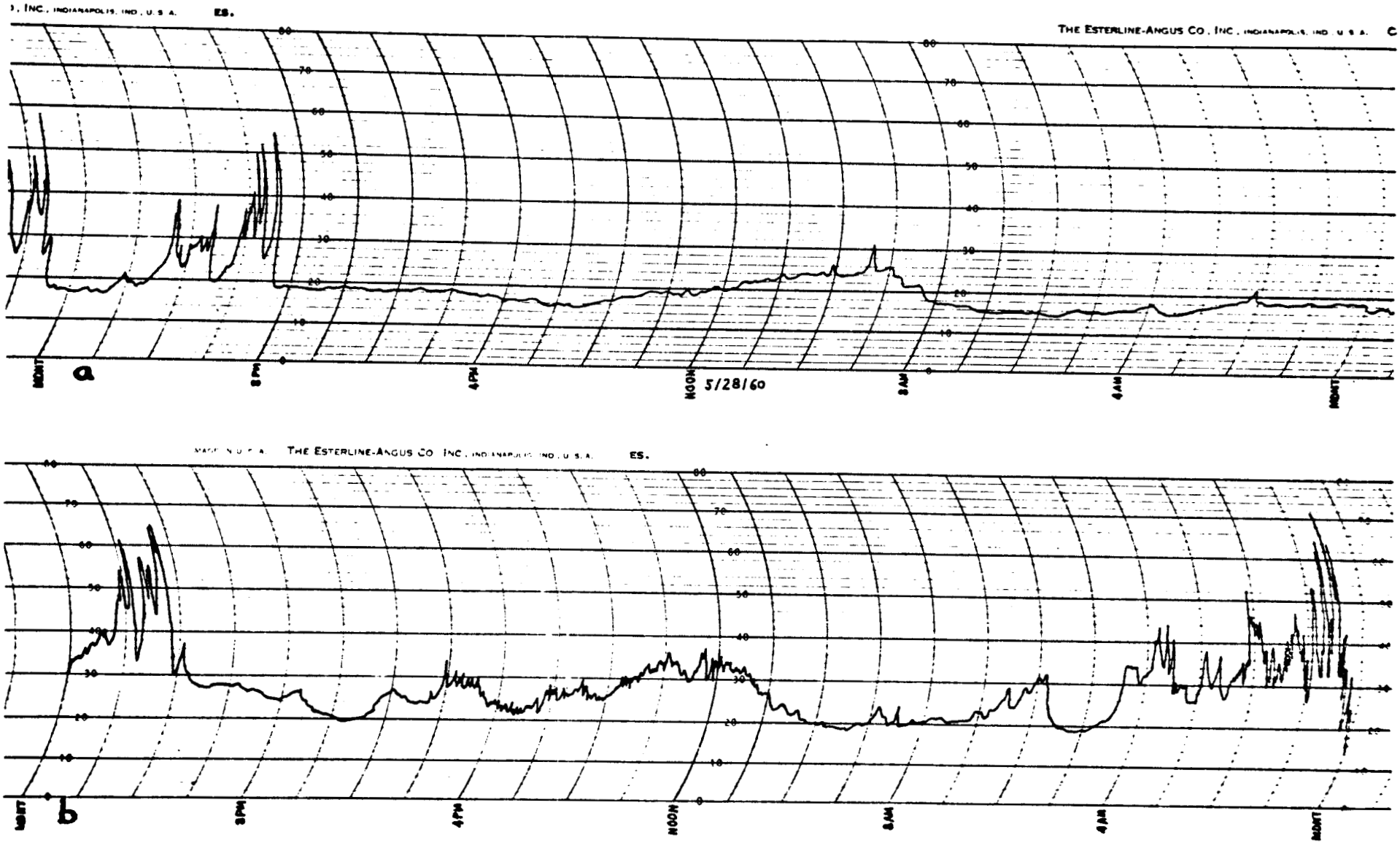

Figure 18

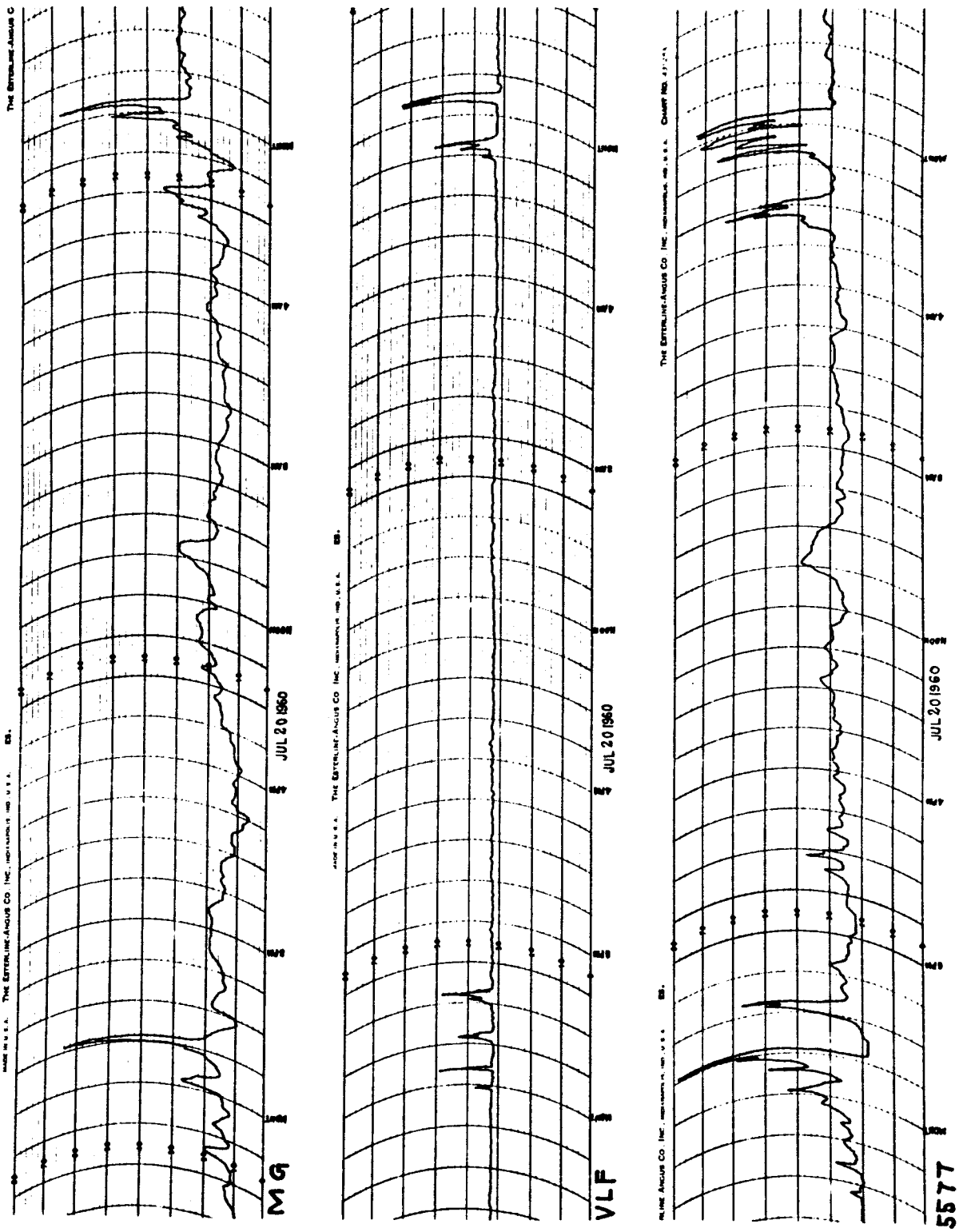

Figure 19

JUL 19 1960 UT

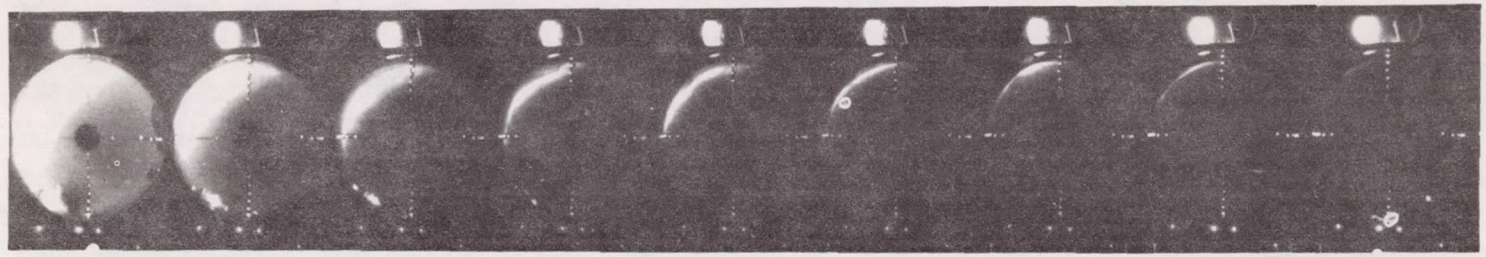

2341 2340 2339 2338 2337 2336 2335 2334 2333

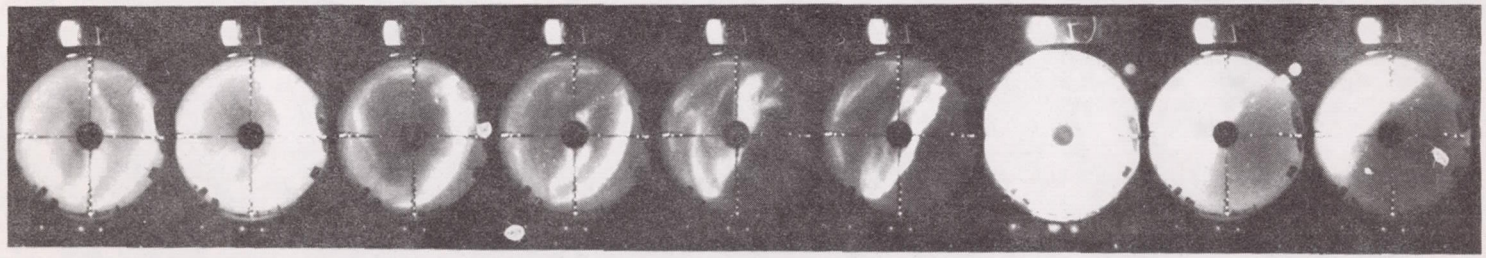

2350 2349 2348 2347 2346 2345 (2344) 2343 2342

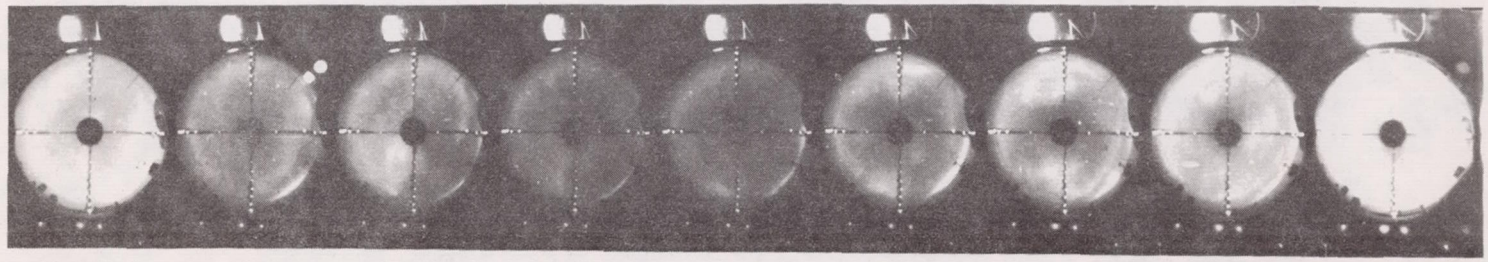

(2359) 2358 2357 2356 2355 2354 2353 2352 2351

Figure 20

JUL 20 1960 UT

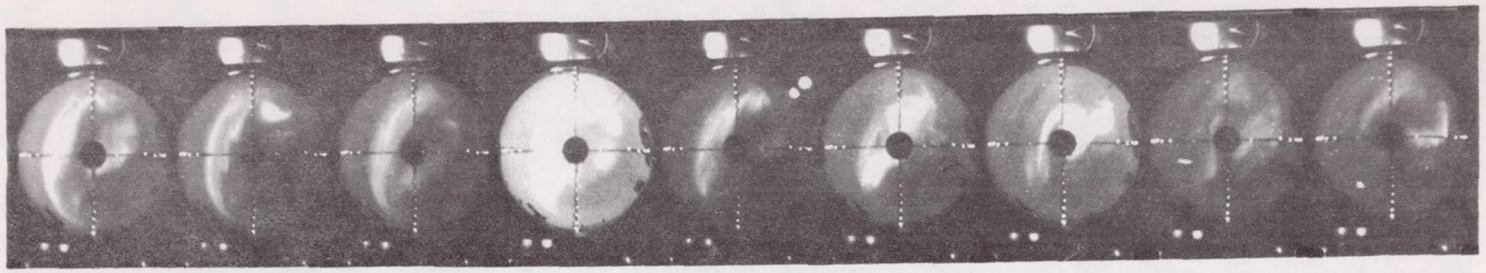

2147 2146 2145 (2144) 2143 2142 2141 2140 2139

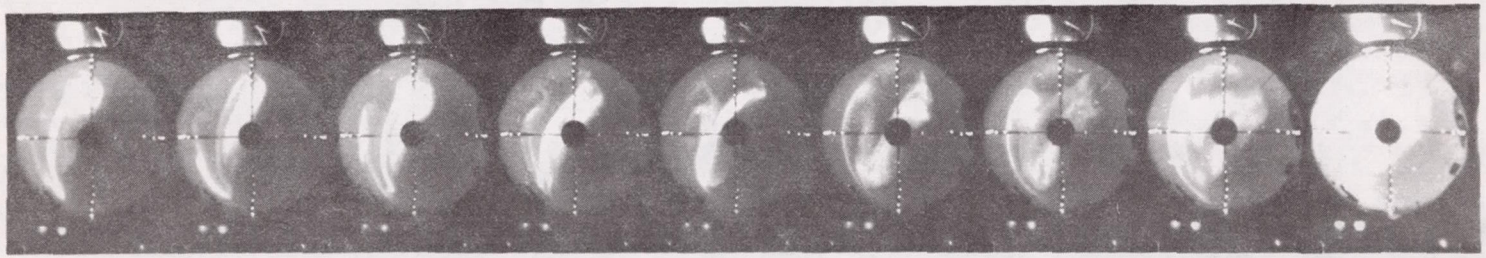

2156 2155 2154 2153 2152 2151 2150 2149 2148

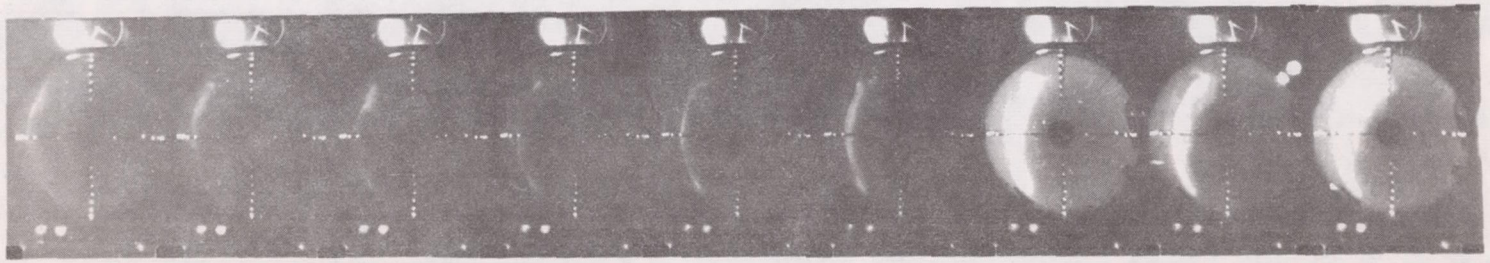

2205 2204 2203 2202 2201 2200 (2159) 2158 2157

Figure 21

JUL 20 1960 UT

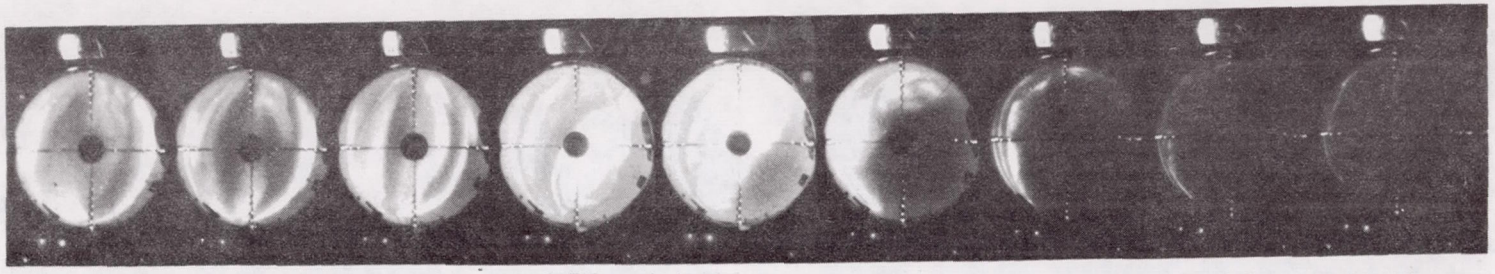

2257 2256 2255 2254 2253 2252 2251 2250 2249

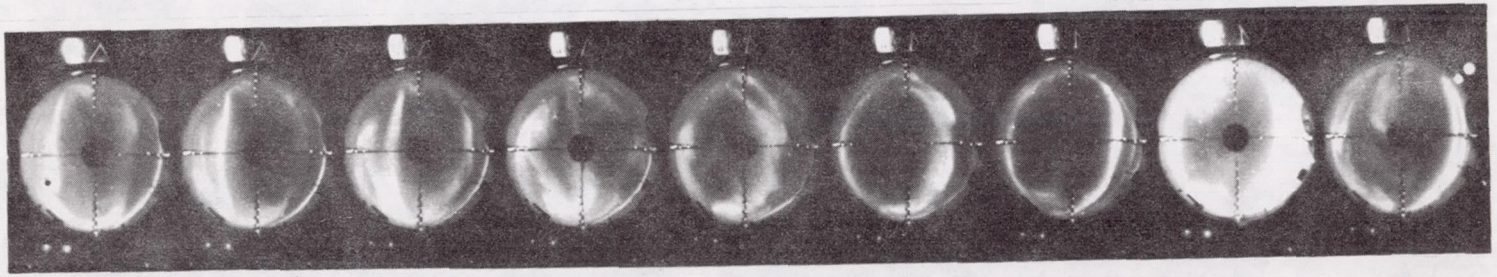

2306 2305 2304 2303 2302 2301 2300 2259 2258

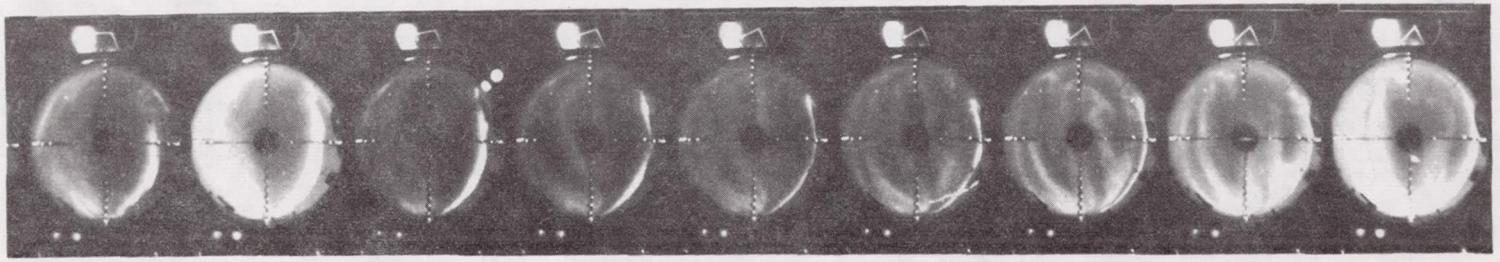

2315 2314 2313 2312 2311 2310 2309 2308 2307

Figure 22

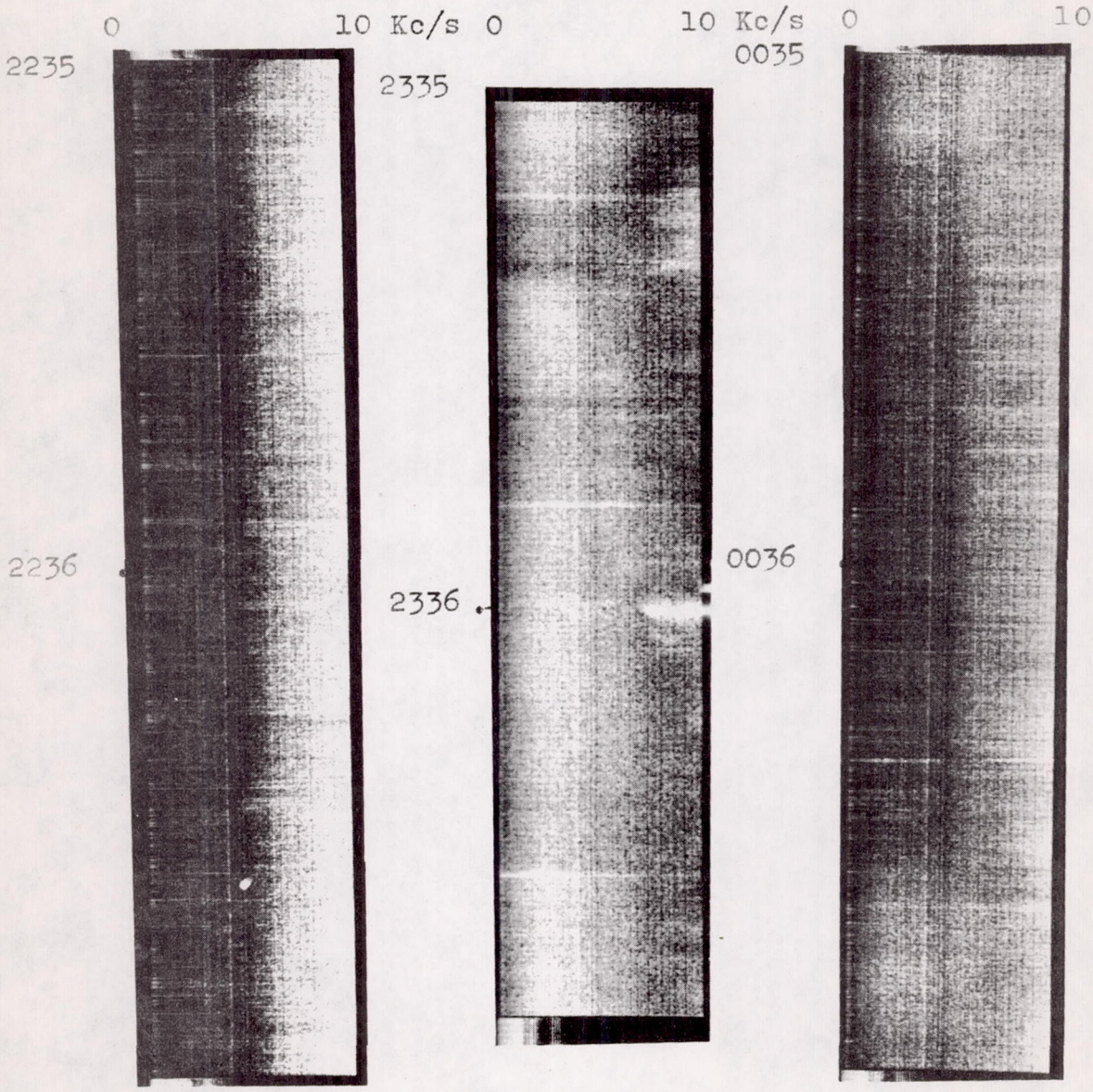

Jul. 19 1960 2235 2335 Jul. 20 1960 0035

Figure 23

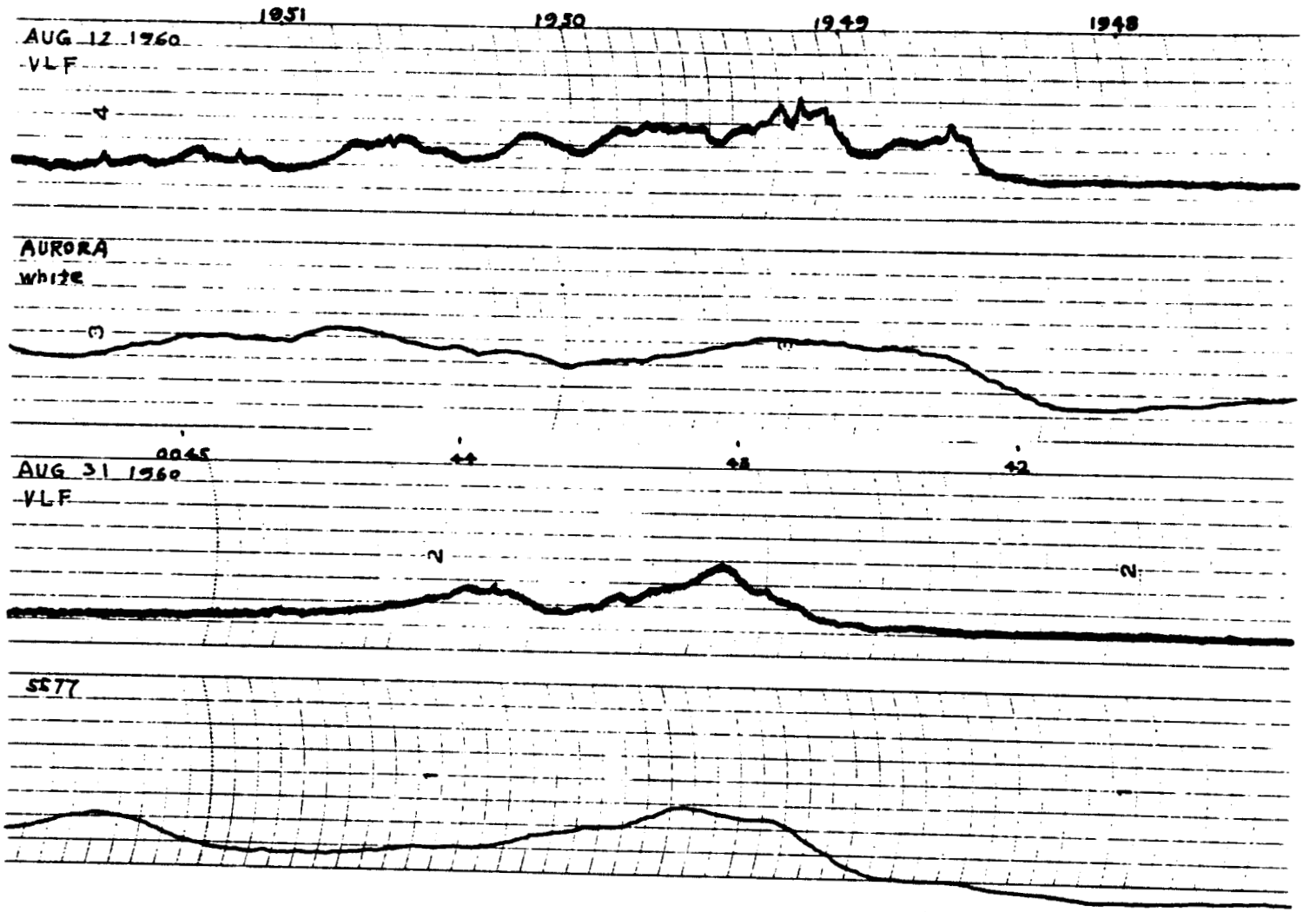
1951
1950
1949
1948
AUG 12 1960
VLF
AURORA
white
0045
44
43
42
AUG 31 1960
VLF
5577

Figure 24

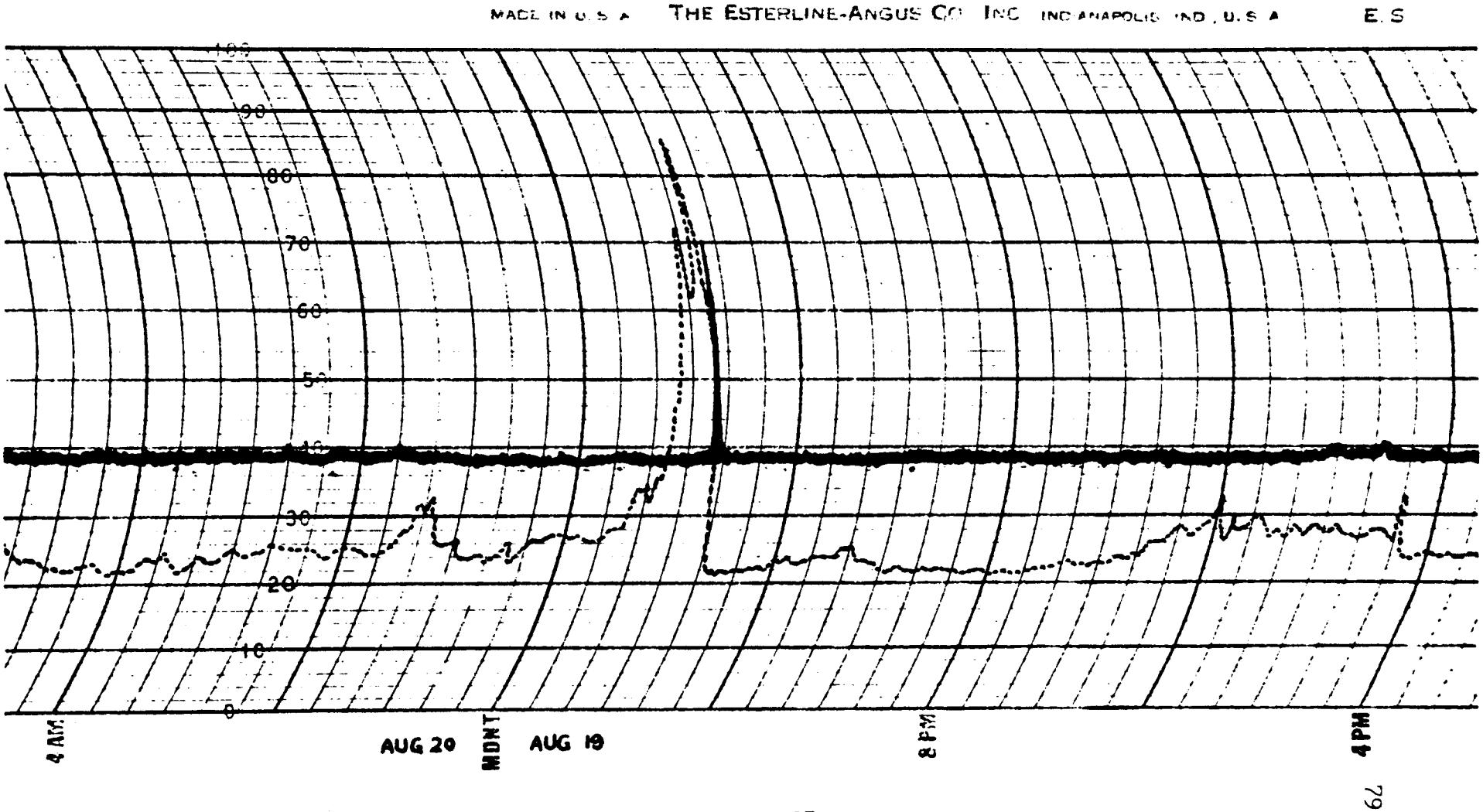
MADE IN U.S.A. THE ESTERLINE-ANGUS CO. INC. INDIANAPOLIS, IND., U.S.A. E.S
100
90
80
70
60
50
40
30
20
10
0
4 AM
AUG 20
MDNT
AUG 19
8 PM
4 PM

Figure 25

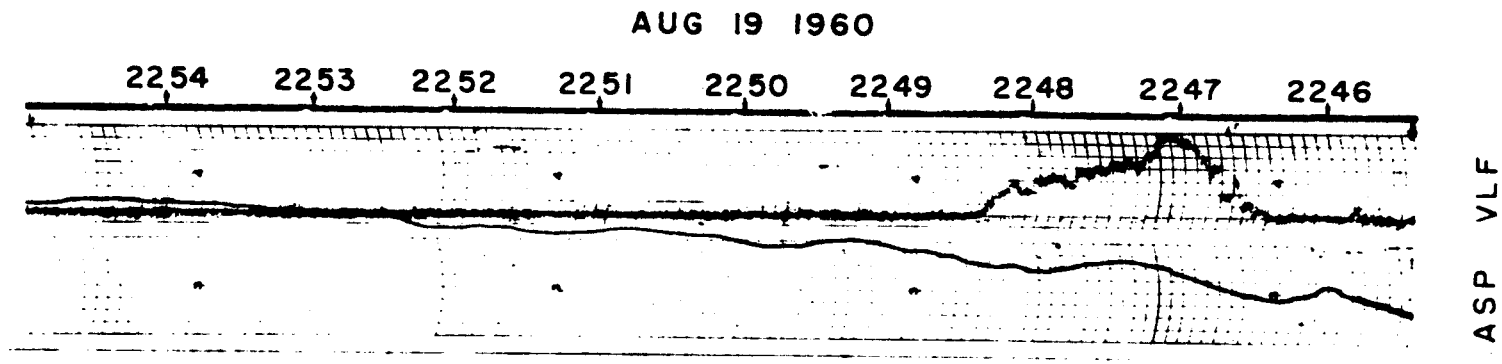

ASP : all sky photometer

Figure 26

AUG 19 1960 UT

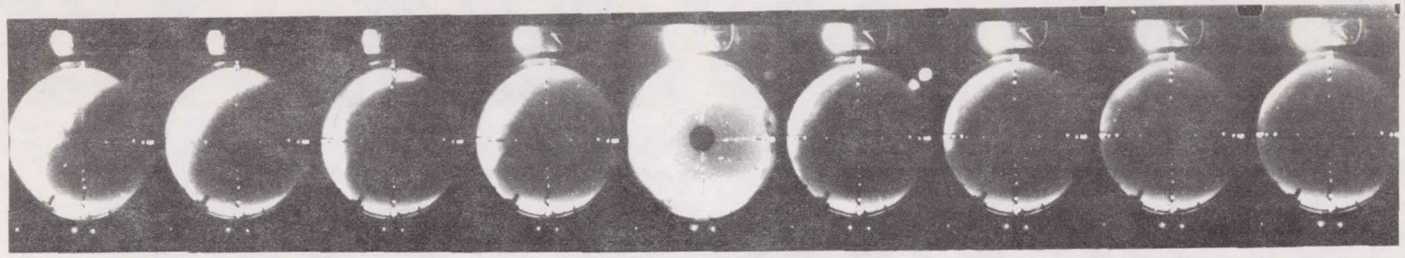

2248 2247 2246 2245 (2244) 2243 2242 2241 2240

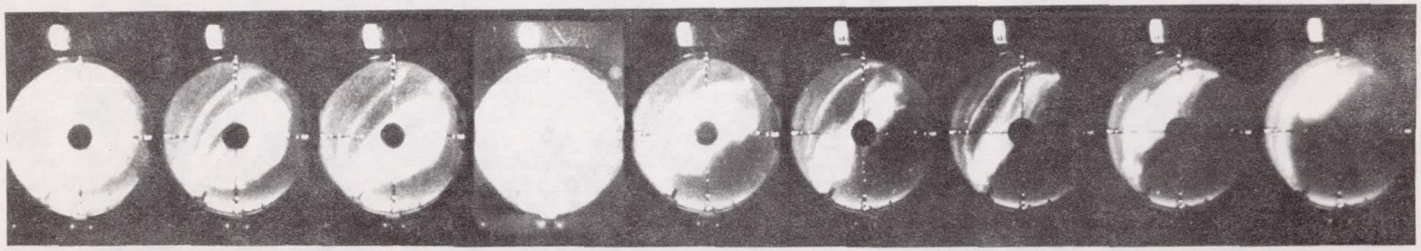

2257 2256 2255 2254 2253 2252 2251 2250 2249

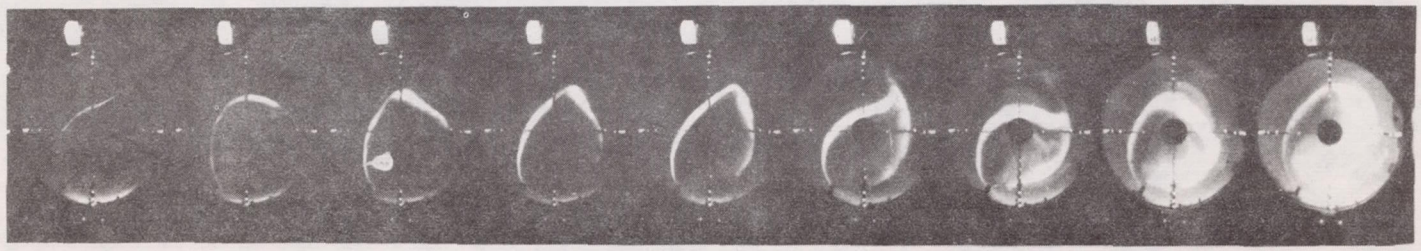

2312 2311 2310 2309 2308 2307 2306 2305 2304

Figure 27

AUG 14 1960 UT

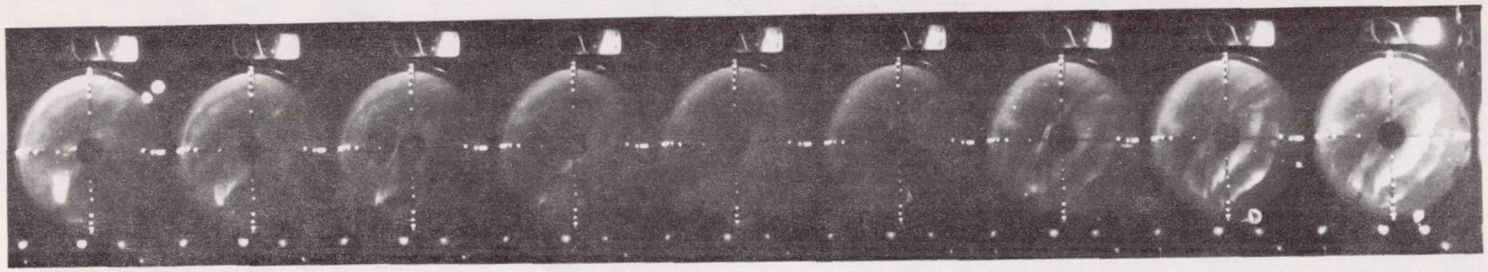

1128 1127 1126 1125 1124 1123 1122 1121 1120

AUG 20 1960 UT

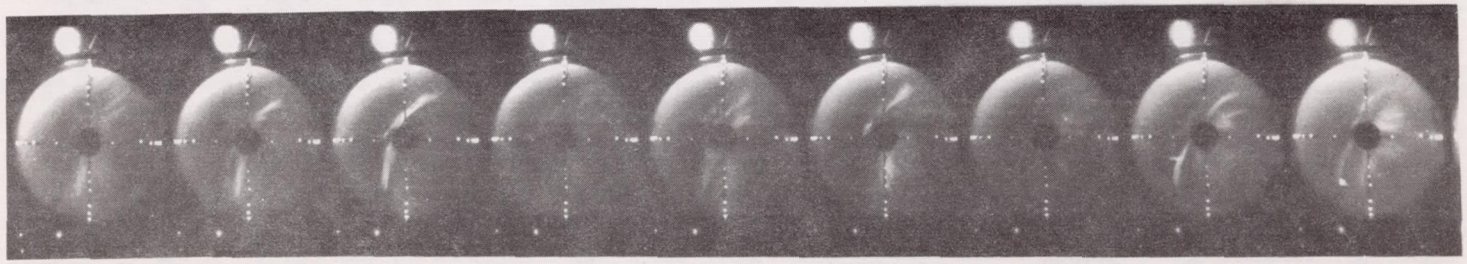

1253 1252 1251 1250 1249 1248 1247 1246 1245

Figure 28

AUG 17 1960 UT

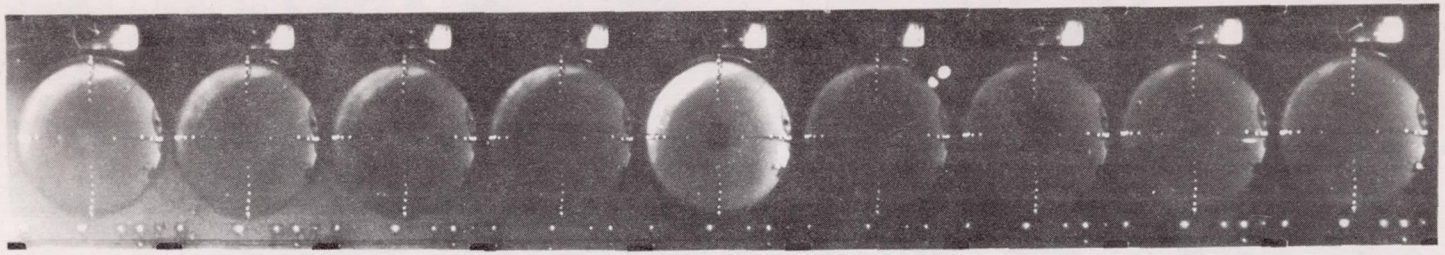

0518 0517 0516 0515 (0514) 0513 0512 0511 0510

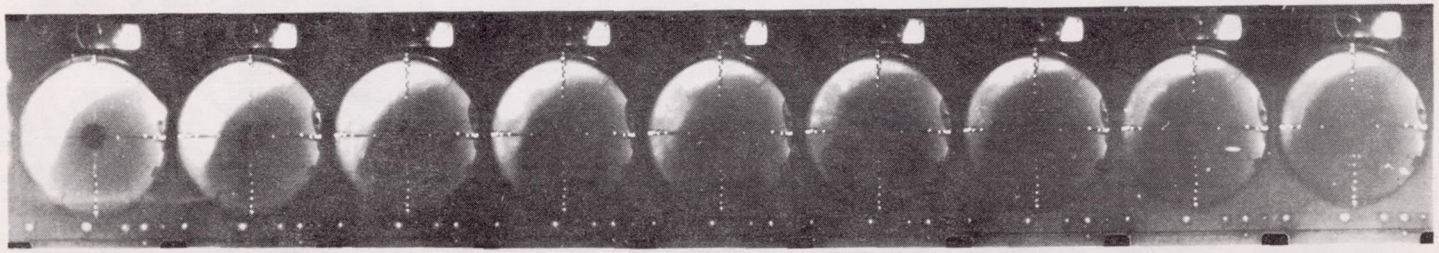

0527 0526 0525 0524 0523 0522 0521 0520 0519

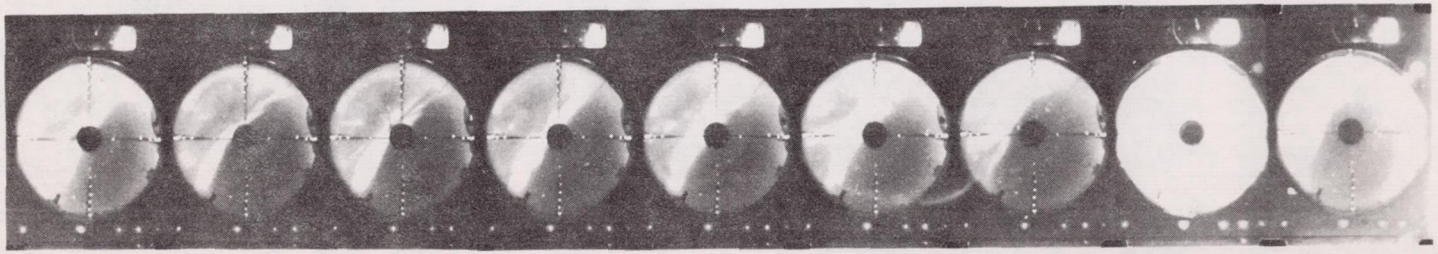

0536 0535 0534 0533 0532 0531 0530 (0529) 0528

Figure 29

THE RELATIONSHIP BETWEEN THE BAND TYPE OF AURORA AND THE GEOMAGNETIC FIELD.

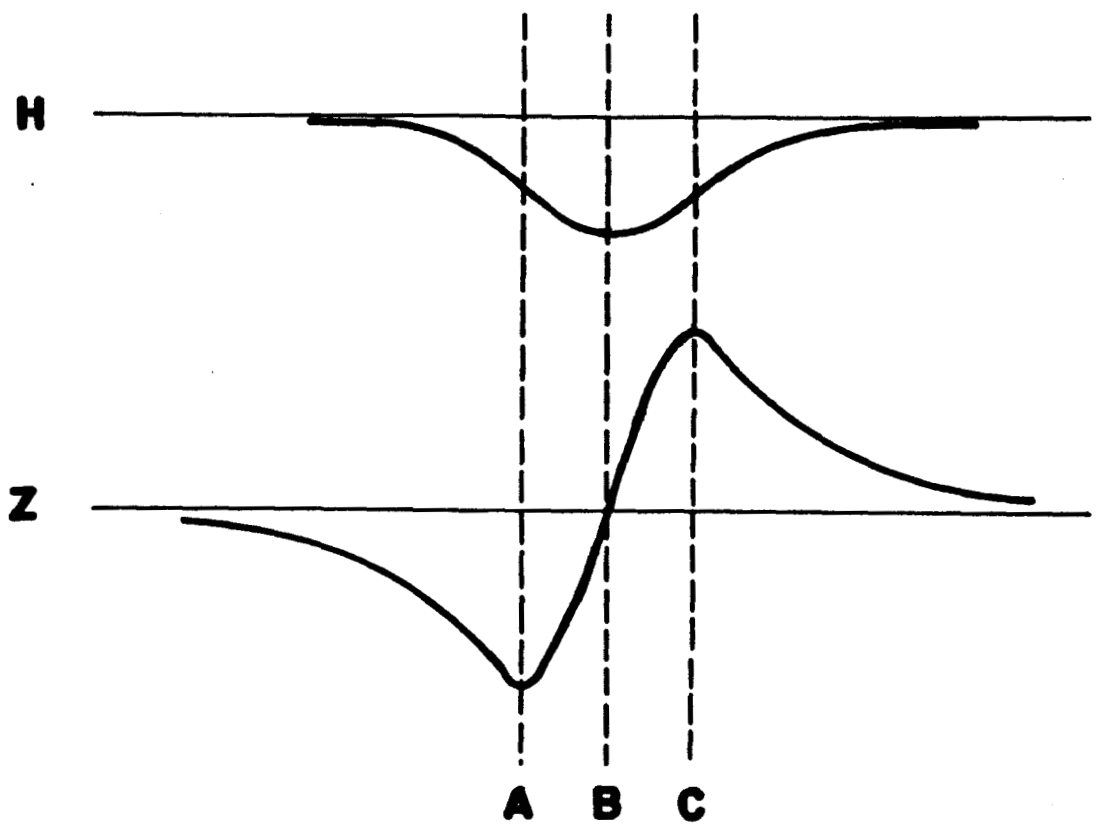

Figure 30

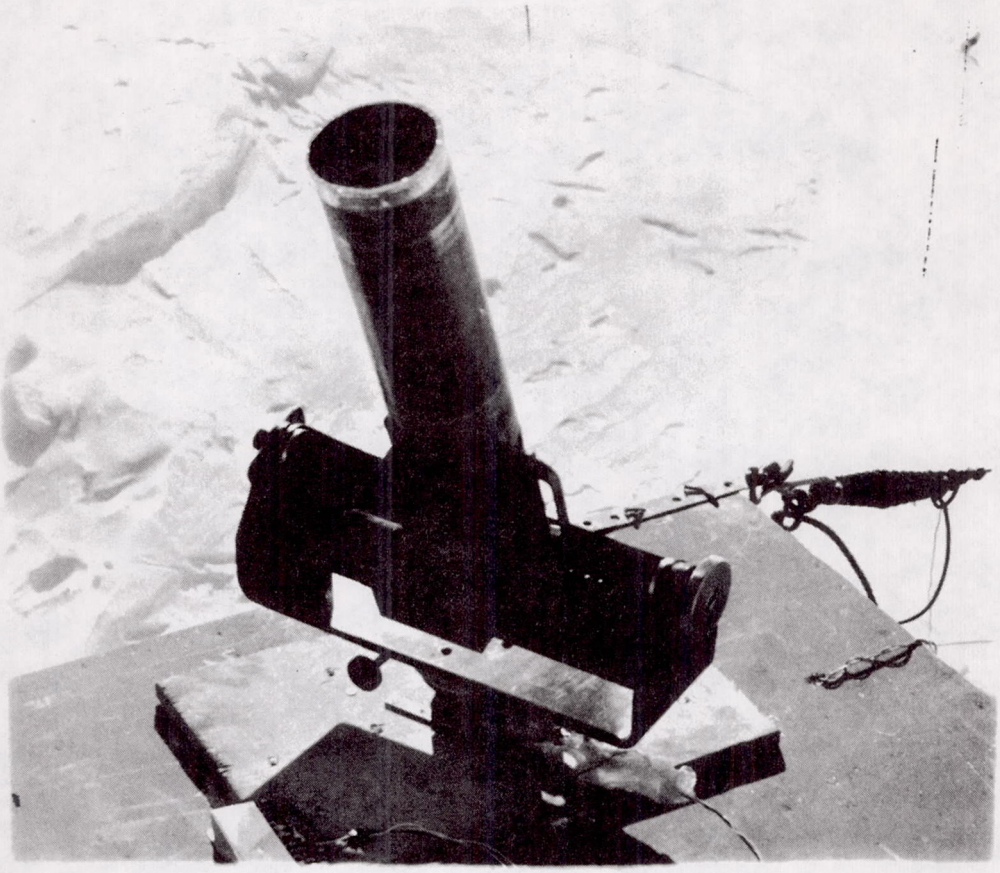

Illustration I

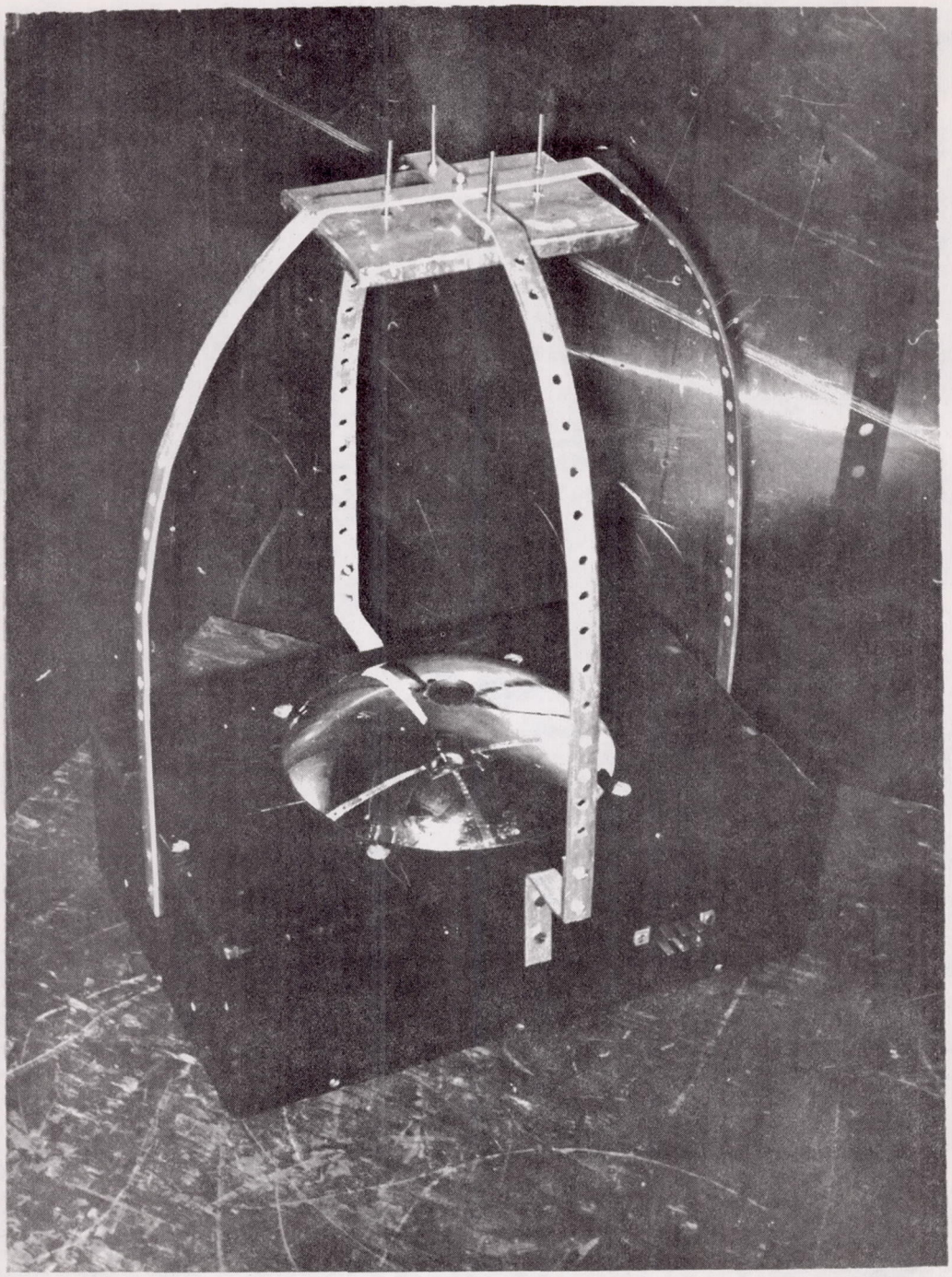

Illustration II

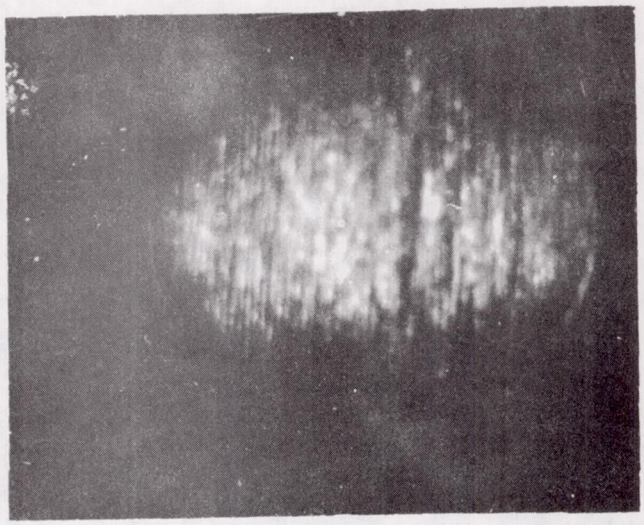

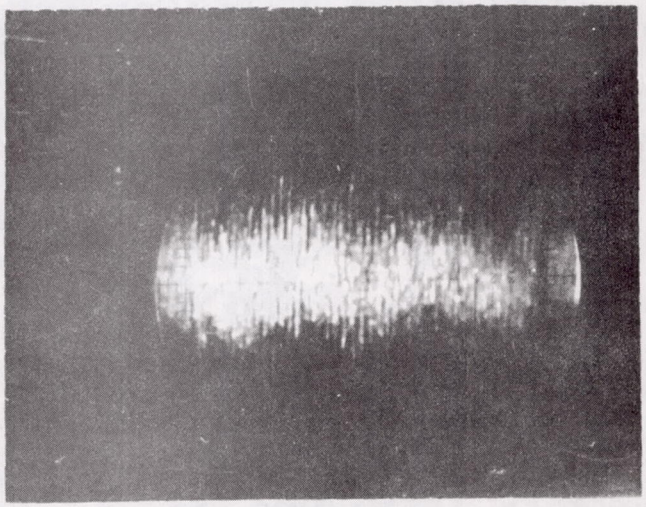

Illustration III